Final Draft
of the original manuscript

Xiong, P.; Dudzinska-Nowak, J.; Harff, J.; Xie, X.; Zhang, W.; Chen, H.; Jakub, M.; Feldens, P.; Macig, F.; Osadczuk, A.; Meng, Q.; Zorita, E.:

Modeling paleogeographic scenarios of the last glacial cycle as a base for source-to-sink studies: An example from the northwestern shelf of the South China Sea.

In: Journal of Asian Earth Sciences. Vol. 203 (2020) 104542.

First published online by Elsevier: 06.09.2020

https://dx.doi.org/10.1016/j.jseaes.2020.104542

Modeling paleogeographic scenarios of the Last Glacial Cycle as a base for source-to-sink studies: an example from the northwestern shelf of the South China Sea

Ping Xiong [a, b, *], Joanna Dudzińska-Nowak [c], Jan Harff [c, **], Xinong Xie [a, b], Wenyan Zhang [d], Hongjun Chen [e], Jiang Tao [a, b], Hui Chen [a, b], Jakub Miluch [a, b, c], Peter Feldens [f], Łukasz Maciąg [c], Andrzej Osadczuk [c], Qicheng Meng [g], Eduardo Zorita [d]

[a] College of Marine Science and Technology, China University of Geosciences, Wuhan 430074, PR China

[b] Hubei Key Laboratory of Marine Geological Resources, China University of Geosciences (CUG), Wuhan 430074, PR China

[c] University of Szczecin, Institute of Marine and Environmental Sciences, ul. Mickiewicza 18, 70-383 Szczecin, Poland

[d] Institute of Coastal Research, Helmholtz-Zentrum Geesthacht, 21502 Geesthacht, Germany

[e] Guangzhou Marine Geological Survey, Guangdong Guangzhou 510760, China

[f] Leibniz Institute for Baltic Sea Research Warnemünde, Germany

[g] State Key Laboratory of Satellite Ocean Environment Dynamics, Second Institute of Oceanography, Ministry of Natural Resources, Hangzhou, China

**Corresponding author at: College of Marine Science and Technology, China University of Geosciences, Wuhan 430074, China*

***Corresponding author at: University of Szczecin, Institute of Marine and Environmental Sciences, ul. Mickiewicza 18, 70-383 Szczecin, Poland*

E-mail address: xiongpingcug@163.com (P. Xiong); jan.harff@io-warnemuende.de

Abstract

Sea-level (SL) data from the Last Glacial Cycle (LGC) have been superimposed on to digital elevation models of the South China Sea (SCS) and adjacent areas, to generate regional paleogeographic scenarios related to 4^{th}- to 5^{th}-order Milankovitch climate cycles. These scenarios—at 123, 65, 60.5, 56, 20, and 0.5 kyr BP—showed that the SCS functioned as an oceanographic interface between the Pacific and Indian oceans during the LGC. A Late Pleistocene paleo-river delta (Hainan delta) offshore west of Hainan Island (China) was an important sediment routing system on the NW shelf of the SCS. To understand the origin of the Hainan delta better, paleo-reliefs of $DEM_{56kyrBP}$ and $DEM_{65kyrBP}$ were reconstructed, using seismic stratigraphy, sedimentology, and back-stripping methods. Geostatistical and geometric models of clinoforms and delta geometry, as well as the courses of the reconstructed paleo-distributary channels and paleo-river valleys, supported the interpretation that most delta sediment could be regarded as erosional products from Hainan Island. We hypothesized that an intensification of sediment supply outpaced SL rise during the Marine Isotopic Stages 4 / 3 transition, resulting in a normal regression during the formation of the Hainan delta. Morphodynamic modeling and meteorological data reanalysis further supported our interpretation that shifts in the Asian Monsoon system—combined with local meteorological effects on Hainan Island and with global SL changes—were the main drivers for the sediment source-to-sink systems at the NW SCS continental margin, during the LGC.

Keywords: Northwestern Shelf of the South China Sea; Hainan delta; sea-level dynamics; paleo-geographic scenarios; East-Asian monsoon system

1. Introduction

The paleogeographic evolution of coastal areas is very important, and has generally been interpreted as representing the results of overlapping driving forces, including eustatic changes, tectonics, isostasy, sediment fluxes, paleoclimate, and the geologic build-up of the coastal zone and its hinterlands (Herbert-Veeh, 1966; Haq et al., 1987; Vail et al., 1991; Peltier 2004; Zhang et al., 2011, 2014; Deng et al., 2017). The NW South China Sea (SCS) is located at a low latitude and had a relatively stable continental margin during the late Quaternary. Therefore, the paleogeographic evolution of the NW SCS is likely to reflect sea-level (SL) change history and sediment supply, and the moderating influence of the glacio-isostatic adjustment (GIA) of the earth's crust (Yin et al., 2019). Meanwhile, the wide shelves of the NW SCS can provide sensitive records of transgressive SL cycles, and represent ideal places for reconstructing paleogeographic scenarios related to the post-glacial period (Hanebuth et al., 2003, 2006, 2009, 2011; Schimanski and Stattegger, 2005; Harff et al., 2013, 2014).

The first approaches to generating paleogeographic maps of the SCS and adjacent areas were published by Sathiamurthy and Voris (2006) and Hanebuth et al. (2011), although these maps temporally covered just the postglacial, and focused spatially on the Sunda Shelf, rather than on the northern SCS. Yao et al. (2009) also reported a series of paleogeographic scenarios, back to 20 cal kyr BP for the NW SCS, which only dealt with geographic changes in the Last Glacial Maximum (LGM). In this study, simplified models superposing digital elevation models (DEMs, DEM_0 from the General Bathymetric Chart of the Oceans (GEBCO_2014) Grid, version 20150318, http://www.gebco.net) with relative sea-level change ($\Delta \mathrm{RSL}_t$) data for both regional and local geographic models, were developed. The regional paleogeographic maps produced by our model were used to exhibit scenarios relating to the development of regional SCS gateways and coastline changes during the Last Glacial Cycle (LGC).

Lobo and Ridente (2014) suggested that global SL data were valuable when restoring the architecture of modern shelf sediments, according to Milankovitch cycles, in areas far away from continental ice sheets, and with insignificant regional (or local) vertical earth crust movements. Regressive deposits are often eroded during the glacial period between Marine Isotopic Stages (MIS) 4 and 2 (from 65–20 kyr BP), however, and—apart from some records from high resolution ice-cores, terrestrial lakes and speleothems samples—the remains of regressive SL systems are usually scarce except some records from high resolution ice-core, terrestrial lakes and speleothems samples (Rea and Hovan, 1995; Steffensen, 1997; Nagashima et al., 2007; Cheng et al., 2016; Sun et al., 2018).

High-frequency Milankovitch cycles are mirrored by sediment architectures in the continental shelf, and can provide a sequence stratigraphy model to establish a stratigraphic framework, analyze depocenter changes, and estimate sediment supply for the paleogeographic evolution of this region (Lobo and Ridente, 2014). By applying this theory, Chen et al. (2016) reported seven seismic reflectors, which represented discontinuities related to SL cycles extending from MIS 5 to the present, offshore of SW Hainan Island (Fig. 1). The direction of the internal progradation reflectors of the Hainan delta (Chen et al. 2015; Feng et al., 2018), and provenance studies on the Cenozoic sediments of Beibu Gulf (Cao et al., 2015; Jiang et al., 2015; Cui et al., 2018) argued that Hainan Island rock erosion could be considered as one of the most important geological processes for this paleo-delta. However, these studies did not discuss factors controlling the formation of the Hainan delta, and the sediment source-to-sink systems at the NW continental margin of the SCS.

In this article, we have contributed to this discussion by combining SL data, DEM data, seismic profiles, and sediment logs from core ZBW drilled by the Guangzhou Marine Geological Survey (GMGS), to generate two paleogeographic scenarios. We believe that our results will help improve understanding of the factors that controlled the formation of the Hainan delta, and reveal how the paleoenvironment—climate, weathering, oceanographic conditions, and so on—evolved in the sediment source-to-sink systems at the NW continental margin of the SCS. We also hope that our study has contributed to the understanding of regional climate conditions in SE Asia during the transition from MIS 4 to 3.

Our paleogeographic scenarios provided background for synoptic analyses of both the Late Pleistocene paleoenvironmental changes to the NW continental margin of the SCS, and the oceanographic dynamics and sediment transport processes of

Beibu Gulf (Zhang et al. 2020).

2. The research area

2.1 Geological setting

Geographically, the SCS is adjacent to South China to the north, the Indochina Peninsula to the west, and is limited by the island chains from Borneo to Luzon to the S and E, respectively. Nowadays, the SCS is connected with the Okinawa Trough through the Taiwan Strait (~ 70 m water depth [WD]) in the north, with the Pacific Ocean through Luzon Strait (2400 m WD) in the NE, with the Sulu Sea through Mindoro Strait (450 m WD) and Balabac Strait (100 m WD) in the E, and with the Indian Ocean through Malacca Strait (30 m WD) in the W (Wang et al., 2009). These interconnections make the geography of the SCS highly sensitive to SL change.

Beibu Gulf is surrounded by Guangxi Province (China) to the N, by Leizhou Peninsula, Qiongzhou Strait, and Hainan Island to the E, and by northern Vietnam to the W. Its slopes are relatively gentle in its northern and western parts, while it is relatively steep along its E slope, where it connects to W Hainan Island. Quaternary sediment in the gulf consists mainly of sedimentary sequences reflecting SL changes, which in turn mirror the climate cycles associated with changes between glacial and interglacial periods, as nominated in the hypothesis first formulated by Milankovitch (1930, 1941). Chen et al. (2015) and Huang et al. (2015) published the first sequence of stratigraphic descriptions for Late Pleistocene sediments in the E Beibu gulf, using seismic survey data and sediment core HDQ2 (Fig. 1).

2.2 The Hainan delta

The Hainan delta was first identified from 2-D seismic profiles, and was defined as a Late Pleistocene proto-delta, covering an area of more than 25,000 km^2 in the offshore Yinggehai Basin, SW of Hainan Island (Chen et al., 2015; Huang et al., 2015). Two wells were drilled for sedimentological studies after the discovery of the delta (see sites LDW and ZBW in Fig. 1), while previous investigations had revealed that it (consisting mainly of muddy-silty sediments) was formed after the MIS 4 SL minimum, when the subsequent SL rise was outpaced by sediment supply from different sources.

2. 3 Oceanography

The changes of surface circulation in the SCS is primarily influenced by the East Asian monsoon and the north-westward Kuroshio Current invading from the north-eastern part of the SCS. In winter, there is a basin-wide cyclonic gyre, named the NW Luzon Cyclonic Gyre, prevailing in the northwestern SCS (Fang et al., 1998). Additionally, it is noticed that a south-westward Guangdong Coastal Current along the northern shelf of the SCS is generated by the winter monsoon (Fang et al., 1998). During summer, mesoscale anticyclonic eddies frequently move along the continental slope from southwest of the Taiwan Island to west of the Dongsha Islands, superposing with the Loop Current and the SCS Warm Current (a separated flow from the SCS Branch of Kuroshio Current) (Hu et al., 2000). The NW Luzon Cyclonic Gyre still exists in northwestern SCS in summer but has reduced and shifted eastward, whereas the NW Luzon Cyclonic Eddy stays approximately at the same position (Fang et al., 1998). On the northern shelf of the SCS, the current systems have completely changed during periods of SL low-stand of the LGC when the Qiongzhou Strait emerged and the Beibu Gulf became a fjord-like embayment.

2.4 Climatic and paleoclimatic condition

The climate and surface circulation of the SCS are mainly influenced by the Western Pacific Warm Pool (WPWP) and the seasonally reversed East Asian monsoon systems. Sea surface temperature (SST) of the SCS ranged from 25.5 °C to 28.9 °C during the MIS 5 and decreased continuously to MIS 4 with the lowest values of ca. 24 °C around 58 kyr BP (Zhao et al., 2006). It is notable that the SST values during the MIS 4.2 (ca. 60 kyr BP) are even lower than those during the LGC (Zhao et al., 2006). The strong SST cooling during the MIS 4 mainly corresponds to Heinrich Event H6, which is observed in many SST records from the Atlantic. The SST values of MIS 3 are generally low, ranging from 26 °C to 24.5°C; which are slightly higher than the SST values of MIS 4.2 (Zhao et al., 2006). During the MIS 2, the SST continues the trend of high-frequency and high amplitude fluctuations before the postglacial warming during MIS 1 starting to govern climatic evolution (Zhao et al., 2006). In particular, the climatic and related sea-level history of the late Holocene (since ca. 6 kyr BP) have caused the formation of the large deltas associated with main rivers in Southeast Asia, including the Red River and the Mekong River.

3. Data and methods

3.1 Sediment data

Sedimentology and depositional age data from sediment core ZBW (site: 17° 10.43′ N, 109° 1.67′ E; water depth: 105 m; core length: 100.75 m) drilled by the

GMGS (see Fig. 1 for location) were used in this study. Seismic reflectors, lithology, and optically stimulated luminescence (OSL) age data are presented in Fig. 2. Hainan delta sediments, as represented in core ZBW, were approximately 48 m thick, and the sedimentological descriptions is as follows: *0–10 m*, sand and silt with shell (Foreshore layer); *10–27 m*, sand and mud containing coarse sand in the sediment bottom, and cross-bedding (Upper–middle shore layer); *27–30 m*, sand and silt, with more sand present than in the upper layers, coarse debris (Delta layer); *30–65 m*, sand and clay, shell debris, cross-bedding (Delta layer); *65–73 m*, silt and clay, massive structure (Delta layer); *73–90 m*, sand and silt, gravel and shell debris (Channel layer); and *90–100 m*, clay and silt (Levee layer).

In this study, deposition age boundaries for Hainan delta sediments, determined using OSL analyses of core ZBW (Feng, 2018a) suggested that the R1 (top delta interface) and R2 (bottom delta interface) horizons were formed at 56 ± 3 and 65 ± 4 kyr BP, respectively (Fig. 2). This indicated that the Hainan delta developed mainly between 65 and 56 kyr BP, which corresponds in geological time to the transition period between MIS 4 / 3.

3.2 Acquisition, processing, and interpretation of seismic reflection data

The seismic data profiles used in our study included both single channel seismic data, measured by GMGS during two RV Fendou 5 expeditions (Chen et al., 2016; Ni et al., 2016), and Parasound data measured by the Leibniz Institute of Baltic Sea Research (IOW), during RV Sonne expedition 219, in 2011 (Schulz-Bull et al., 2012). The seismic lines were recorded on the Chinese part of Beibu Gulf, without the

Vietnamese margin (Fig. 1). Details of these seismic data may be found in the Method Details.

Reflectors R1 (56 kyr BP) and R2 (65 kyr BP) were identified using strong seismic reflection characteristics and sediment lithology. These reflectors, as well as the sea floor reflector (R0), were revealed in the profiles from the seismic data using IHS KINGDOM software. The margin-wide surfaces of discontinuity (R0, R1, and R2), which were traced from the shelf break to the inner shelf, were identified based on analysis of the reflection terminations, and define the major seismic units (SUs). Time-depth conversions were calculated using unit thicknesses measured on both seismic profiles and the ZBW core. Sound velocities of 1577 and 1635 m / s were assumed for sediment SUs (R0–R1) and (R1–R2), respectively (Miluch et al., 2020, this issue).

Following conversion to metric, SU (R0-R1) and (R1-R2) thicknesses were estimated using Golden Software Surfer, with the universal kriging model (Olea, 1999) applied by using Golden Software Surfer (Yang et al., 2004) to generate the thickness models. The sediment mass calculation algorithm was also applied, and more detail on the application of these methods is available in the Method Details.

3.3 The paleogeographic GIS-based Model

In this study, the broad purpose of the paleogeographic GIS-based model was to display the changes in a reference digital elevation model, DEM_0, including the marine and terrestrial research area, during a time span, Δt. This time span included differences in the paleogeographic scenarios active from 0 (present time) to 123 kyr

BP (MIS 5 SL high). DEM_0 was created from existing GEBCO database digital elevation data, with a 30 arc-seconds resolution. For the regional SCS scale data, we used GEBCO_2014 grid data, extending from 95° E, 10° S to 128° E, 27° N, and for the local scale of the NW SCS, we integrated seismic and multi-beam data which extended from 104° E, 14° N to 115° E, 23.5° N. The general paleogeographic, GIS-based model has been explained in more detail in the Method Details.

Data on relative SL changes at continental margins are available globally for the post-glacial period, while regional SCS SL reconstructions covering the Last Glacial Cycle (LGC) are not. SL data published by Waelbroeck at al. (2002) have been widely used to cover the last 430 kyr BP in the literature. Using DEM_0 and selected global SL data from Waelbroeck et al., 2002, we generated paleogeographic scenarios related to seven relative SL maxima and minima. All SL data are listed in Table 1 and shown in Fig. 3. The date of the MIS 4 SL minimum and the age of reflector R2 were too close to be separated, according to the confidence intervals of the data, so we used data for reflector R2 to represent the MIS 4 SL minimum.

The back-stripping method (Allen and Allen, 2008) was applied in this study to obtain paleogeographic scenarios at 65 kyr BP (MIS 4 SL minimum and the onset of Hainan delta formation) and 56 kyr BP (MIS 3 / R1 SL maximum and Hainan delta top truncation). The back-stripping method was also required for reconstructing paleo channels, and for morphodynamic numerical experiments (Zhang et al., 2020), with additional detail provided in the Method Details.

We simplified the procedure by only considering Beibu Gulf bathymetry variation, using stepwise removal of thicknesses—($\Delta SED_{R0\text{-}R1}$) for sediment unit (R0–R1), and ($\Delta SED_{R1\text{-}R2}$) for sediment unit (R1–R2)—to reconstruct Beibu Gulf paleo-relief at 65 kyr BP (MIS 3 / R1 SL maximum) and 56 kyr BP (Hainan delta top truncation), respectively. GIS-layers representing $\Delta SED_{R0\text{-}R1}$ and $\Delta SED_{R1\text{-}R2}$ thickness models were generated using the geostatistical methods described in the Method Details.

3.4 Circulation model

Simulation results from a three-dimensional circulation model which has been successfully applied to the SCS (Chen et al., 2016, 2019; Zhang et al., 2016a, 2016b, Yin et al., 2019) are used to investigate the paleo-oceanographic circulation patterns in our study area. The circulation model contains two major functional modules: (a) A 3-D circulation module based on the Princeton Ocean Model (Blumberg and Mellor, 1987; Mellor, 2003) adopting the fourth-order vertical pressure gradient scheme from Mccalpin (1994) to better resolve hydrodynamics over complex topography characterised by sharp bathymetric gradients (e.g. around seamounts and above shelf breaks), and (b) A bottom boundary layer module adopting a quadratic drag relationship (with a constant drag coefficient 0.0025) between bottom current velocity and bed shear stress. The readers are referred to the Method Details for details of the model setup and parameterizations.

4. Results

4.1 Paleogeographic reconstructions of the SCS and the NW SCS during the LGC

In the work described in this paper, we reconstructed paleogeographic scenarios for the entire SCS on a regional scale, before generating local-scale scenarios for its NW shelf, based on the GIS-based model described in Section 3.3. Due to lack of comprehensive data coverage, site-specific sediment accumulation thickness during the LGM and vertical crustal movement rates were not considered for the regional-scale reconstruction. NW SCS paleogeographic scenarios were also reconstructed, using the DEM and global SL change data. The paleogeographic reconstruction during the LGC can be seen in Figs 4 and 5, which illustrate the paleogeography, at regional and local scales, for 123 kyr BP (MIS 5 SL maximum), 65 kyr BP (MIS 4 SL minimum (R2)), 60.5 kyr BP (MIS 3 SL maximum), 56 kyr BP (MIS 3 SL maximum (R1)), 20 kyr BP (MIS 2), and 0.5 kyr BP (MIS 1).

4.1.1 SCS paleogeographic scenarios during the LGC (MIS 5–1)

During the Last Interglacial Period (MIS 5), the relative SCS SL was ~ 6.5 m higher than the present-day level (Fig. 3; Table 1). The SCS continental shelf was wider than now, and the deep basin water depth averaged ~ 4700 m (Fig. 4a). The Malacca, Balabac, Mindoro, Luzon, and Taiwan straits were wider, which resulted in the SCS being a relatively open sea (Fig. 4a). The SCS expanded largely because of rising SL, which rose at rates of up to 135 m / kyr over the period from MIS 6 to MIS 5. Under these conditions, the SCS coastline retreated, and many lagoons and islands developed. The rising SL also caused the coastal plains and river deltas of Vietnam and Thailand to be completely submerged, and the continental shelf expanded by > ~ 1×10^5 km^2.

During the MIS 4 SL minimum (65 kyr BP), the SL dropped by 91.15 m, to a point ~ 84.65 m lower than the present-day level. The NW SCS continental shelf was exposed as a coastal plain, and was unaffected by any marine influence (Figs 4b and 5b). Our reconstructions showed that the SCS connections to the Indian Ocean to the south and the Okinawa Trough to the north were closed, and that the SCS was only connected to the Pacific Ocean through the Luzon Strait. As the Qiongzhou and Taiwan straits were closed, Hainan and Taiwan islands were contiguous with the South China mainland. Sunda Shelf and Beibu Gulf were exposed, and eroded in terrestrial environments, generating many buried paleo-channels and subaqueous deltas in the W SCS. These channels and deltas were covered by younger sediments during the later high SL stages and were imaged on our seismic profiles. Large rivers, such as the Mekong and Red rivers, supplied terrestrial sediments further seaward, all the way to the shelf slope break. Our results also showed that the Indochina and Malay peninsulas, and the islands of Sumatra, Kalimantan, and Java, were united into a single landmass, making the SCS a continental sea during the MIS 4 SL minimum.

As the glacial period ended, the SL rose again, reaching a level 48 m lower than the present-day during MIS 3. A fast transgression occurred in the SCS, and the coastline retreated quickly, to the point where, as shown in Fig. 4c, the rising sea submerged Sunda Shelf and Beibu Gulf. At this point, the shoreline retreated to more than half of the present-day continental shelf width, and then, after the de-glacial period in MIS 3, the SL fell again, reaching a level 56 m lower than the present-day, at the time of R1. At this time, coastal areas such as the Red and Mekong river estuaries were exposed, developing several paleochannels (Fig. 8a). The SCS was still small, and was only open to the Western Pacific Ocean due to the connection between the Malay Peninsula and Sumatra.

The time of R1 sediment formation (56 kyr BP) was a period of relatively high SL in MIS 3, with an SL 55.90 m below the present-day level (Table 2). The paleogeographic characteristics at 56 kyr BP were similar to those in MIS 3, and the ocean was approximately the same size (Figs 4c and d). The north and south parts of the Taiwan Strait were not completely open, and Taiwan Island was still connected with the South China mainland. At this time, the area of Beibu Gulf decreased, and the coastline retreated to the W margin of Hainan Island. The Gulf of Thailand was a saltwater lake, and was probably not connected to the SCS, while Sunda Shelf shrank back, and its coastline became complex, with many islands, fjords, and lagoons. During this period, as in MIS 3, the Red and Mekong river deltas were located more than 150 km further offshore than now.

During the LGM, the SL declined rapidly again. We reconstructed the MIS 2 (20 kyr BP) paleogeographic scenario, when the relative SL was ~ 123 m lower than present, to characterize the geomorphology of the SCS at the lower SL of the LGM (Fig. 4e). The results showed that it had adopted a diamond-shaped geometric character, being connected with the Western Pacific Ocean through Bass Strait. At this time, the SCS had no shelf, with the present-day shelf (Fig. 4f) totally exposed as a coastal plain, through which the Red, Mekong and Menam rivers transported sandy and argillaceous materials to the shelf slope break—and even out to the abyssal plain.

During MIS 1, the SL rose until achieving its present-day level. The paleogeographic scenario for this period showed that the SCS extended from NE to SW, and formed a rhomboid deep basin (Fig. 4f); at this time, almost all straits were open again, and the SCS manifested as a semi-closed sea, connected to the Okinawa Trough in the north, the Pacific Ocean in the NE, and the Sulu Sea in the SE. The SCS boundary was restricted by the continental margin and a series of islands of different sizes and shapes. The west, south, and north parts of the SCS were close to the continental shelf of Asia and exhibited slow water depth changes. In the E SCS, the Manila Trench developed, with a dramatic water depth change, while the width of the continental shelf on the north and south sides reached nearly 300 km, being narrower on its W side, at < 100 km. The outer continental shelf had a series of seamount chains, submarine canyons, and underwater deltas.

4.1.2 Paleogeographic scenarios for the NW SCS during LGC (MIS 5–1)

During MIS 5, the NW SCS relative SL was approximately 6.3 m higher than the present-day, and most coastal plains were submerged (Fig. 5f). Changes to the coastline, and to topographic features of the NW SCS, were minor, however, low altitude areas, including most of the Pearl River delta, Nanliu River, and the Qinjiang delta, were submerged. Beibu Gulf occupied an area of approximately 2.5×10^4 km^2 and exhibited a relatively flat submarine topography. The shelf slope-break, at the 125 m isobath, showed a N–S trend in Central Vietnam, and a NE–SW trend in SE Hainan Island, shifting to an ENE–WSW trend in offshore Guangdong province, where a slope-break distribution pattern similar to the present-day existed. Water isobath patterns in the Yinggehai Basin were convex to the NW, with an axis trending NW–

SE, revealing deeper water in the center, with shallower depths at the sides. In contrast, Beibu Gulf isobaths changed very little, probably indicating a flat submarine geomorphology. The sea deepened rapidly at the shelf break, and the Xisha (Paracel Islands) were completely submerged.

The R2 reflector (65 kyr BP) represents a sequence boundary with low frequency and strong amplitude reflection characteristics. It is not only a sedimentary sequence interface but also an important geological time boundary at the lowest MIS 4 SL (85.65 m below present-day SL), representing the bottom layer of the Hainan delta. The paleogeographic scenario of this period was crucial for analyzing the formation and evolution processes of the Hainan delta, and discussion of the response relationship between the paleogeomorphology and sedimentation. The SE Yinggehai Basin was a shallow shelf, while its NW and north parts were land areas with an altitude of < 80 m, representing typical offshore plain and river delta plain environments. At this time, Hainan Island elevation ranged from 150–300 m, and may have suffered from strong denudation.

During MIS 3, the relative SL rose again, and our DEM results showed that the Beibu Gulf coastline was 50–100 km inland from the present coastline (Fig. 5c). Beibu Gulf surrounded Hainan Island with a C shape, while the island itself was connected with continental South China, and was the highest topographic feature in the NW SCS, therefore playing a major role in the development of the Hainan delta in the NW SCS continental shelf.

The R1 reflector formation time was at 56 kyr BP, representing another important stratigraphic interface sequence between interglacial MIS 3 and glacial MIS 2. During this period, the relative SL was 55.90 m lower than the current sea level, and 4.60 m lower than the MIS 3 maximum sea level. Beibu Gulf shrunk noticeably and showed a remarkable coastline migration (Fig. 5b), which was either a response to the relative SL drop, or was associated with a Red River delta precursor. The north and south parts of Taiwan Strait were still not completely opened, and Taiwan Island was still connected to the South China mainland. In this period, Beibu Gulf shrank and the coastline retreated to the W margin of Hainan Island. The Gulf of Thailand was a saltwater lake, probably unconnected to the SCS, while Sunda Shelf shrank, creating a complicated coastline, with many islands, fjords, and lagoons.

In the MIS 2 glaciation period, the relative SL decreased sharply, to a level approximately 123 m lower than present-day, and the NW SCS regressed. Our work showed that the NW SCS was mainly characterized by continental shelf slopes and abyssal plains during this period, with a depth of > 1000 m (Fig. 5a). The shelf extended NE, and was narrower (< 15 km), revealing significant contraction compared to the interglacial period.

During MIS 1, the SL rose again, until ~ 6 kyr BP, and has since remained relatively stable at the present-day level. Details of the Holocene sea-level regression after 6 kyr BP were investigated by Groh and Harff (2020). Our study has shown that one effect of SL rise was the opening of Qiongzhou Strait, separating Hainan Island from Leizhou Peninsula (Yao et al. 2009).

4.2 Reconstruction of paleogeographic scenarios for the MIS 4 SL minimum (R2) and

MIS 3 SL maximum (R1), in the NW SCS, by back stripping

4.2.1 Sediment units (R0–R1) and (R1–R2) thickness maps

The thickness map of $\Delta SED_{R0\text{-}R1}$ identified Late Pleistocene (MIS 3–present) terrestrial and Holocene marine sediments. We found that $\Delta SED_{R0\text{–}R1}$ was mainly distributed to the W and S of Hainan Island, with a value of < 30 m. It was bordered by the coastline of the MIS 3 (R1) SL maximum, representing the onset of regressive sediment accumulation (Fig. 6a). The thickness map (Fig. 6a) shows two depocenters; one with a maximum thickness > 60 m was located in SE Beibu Gulf, close to the shelf break, and consisted mainly of Late Pleistocene–Holocene marine sediments. The other, with a maximum thickness > 50 m, was to be found to the W of Hainan Island, and consisted of Holocene marine sediments, representing the so-called "Southern Beibu Gulf Mud Depocenter" (Ni et al., 2016). Holocene marine sediments with insignificant thickness (< 5 m) on the shelf outside the MIS 3 (R1) coastline have not been discussed in this paper.

$\Delta SED_{R1\text{–}R2}$ records the SL history between the MIS 4 SL minimum and the MIS 3 SL maximum; we found that it was bounded by unconformity (reflector R2) at the bottom, marking the erosional surface of the MIS 4 SL minimum. At the top, it was bound by reflector R1, which indicated the SL fluctuation (flooding surfaces) during the MIS 3 SL maximum. The distribution and extension of $\Delta SED_{R1\text{–}R2}$ was seen to substantially increase, which was consistent with the distribution of the ancient coastline in MIS 3, especially extending northwards to the W and N margins of Hainan Island.

We found that $\Delta SED_{R1\text{-}R2}$ was spatially distributed around Hainan Island in a c-shaped formation. Areas showing a thickness > 10 m were found over > 80% of the whole area, with thicknesses > 30 m found over > 50%. A sediment layer > 40 m thick was distributed to the S of Hainan Island, in a pillow-shaped formation, reaching its maximum thickness of > 60 m. Overall, sediment layer thickness here increased from the NW to the SE, with its depocenter at the intersection of the Yinggehai–Qiongdongnan basins, on the S side of Hainan Island. We found that this depocenter had moved, since 65 kyr BP, from the north to the south and gradually away from Hainan Island. As shown in Fig. 6b, $\Delta SED_{R1\text{–}R2}$ had two Late Pleistocene depocenters—one being the Hainan delta in the SE, and the other a fan formed to the W of Hainan Island—which were interpreted as being relicts of the paleo Red River delta. In terms of sequence stratigraphy, both $\Delta SED_{R0\text{–}R1}$ and $\Delta SED_{R1\text{–}R2}$ were regarded as "Para-sequences", based on the definitions proposed by Van Wagoner et al. (1988, 1990).

4.2.2 $DEM_{56kyrBP}$ and $DEM_{65kyrBP}$ reconstructed by back-stripping

Using the results from Section 4.2.1 on sequence stratigraphic interpretation, sediment unit thickness calculations, and stratigraphic back-stripping correction, our research focused on reconstructing MIS 3 (R1) SL maximum ($\mathrm{DEM_{56kyBP}}$), and MIS 4 SL minimum ($\mathrm{DEM_{65kyBP}}$) paleogeographic scenarios for the NW SCS (Fig. 7).

During MIS 3, as depicted in Fig. 7a, the geographic character of Beibu Gulf changed; its depth to the W of Hainan Island was < 5 m, and a small submarine trough, with a depth of 30–40 m was seen to occur in the Yinggehai area, SW of the island.

This trough expanded in the sea transition zones on the W and SE sides of the Yinggehai and Qiongdongnan areas, deepening to > 60 m.

The paleo-DEM$_{65kyrBP}$ map (Fig. 7b) reflects the geographic characters of the Hainan delta before it began to develop. During this period, the coastline extended as far north as the NW of Hainan Island, and as far west as the Vietnamese outer shelf, allowing the Yinggehai area to expand to at least three times its previous size.

The paleogeographic features of the NW SCS changed from the MIS 4 SL minimum to MIS 3(R1) SL maximum. With the rise in relative SL, the coastline retreated significantly in the south Chinese and Vietnamese continental margins, except in the Hainan Island vicinity. In contrast, the "depression" of the MIS 4 SL minimum was absent from the S of the Yinggehai Basin during the MIS 3(R1) period, indicating that the formation of the Hainan delta had significantly changed the NW SCS morphology.

Using information concerning paleo-rivers extracted from seismic data, and from the paleo-valleys network from the DEM for the NW SCS, we reconstructed the river networks extant at 56 kyr BP. As shown in Fig. 8a, the South China continental shelf and Hainan Island shelf had different river systems. There were large, N–S trending river systems in the north part of the Beibu Gulf, NW–SE trending river systems in the south part of the Beibu Gulf, E–W and NE–SW trending river systems in the northern margin of Vietnam, an underwater channel system from NW–SE in the Yinggehai Basin, and a N–S, independent underwater channel system in the south central part of the Yinggehai Basin.

Different types of river systems in different regions may have reflected the connection between terrigenous provenances (source regions) and the N–W SCS basins. In particular, sediments from Hainan Island and the Vietnamese margin (including the Red River system) could both contribute to the Hainan delta. Several erosional incisions identified by Miluch et al. (2020, this issue) are also shown in Fig. 8, where the obtained patterns show that R2 channels were mainly directed to the western depocenter of the Hainan delta, whereas the R1 channel system was more extensive, covering a large part of the shelf area. The observed spatial distribution of the incised valleys supported an eastward shift in the river drainage systems during the low SL periods responsible for the R2 and R1 discontinuities.

The R2 system, consisting of 9 channels, was less developed compared to the R1 system, with 20 identified channels, and this difference may be explained by eustatic changes. The R2 system was developed during low SL periods; the relative SL curve proposed by Waelbroeck et al. (2002) indicated that after 65 kyr BP, SL rise accelerated compared to the period between 56 and 65 kyr BP. The marine transgression which followed the formation of R2 shortened the time during which the channel system could develop. E Beibu Gulf remained submerged, which explained the lack of valleys there. After 56 kyr BP and the formation of R1, the SL began to decrease (albeit with two periods of slight increases) until the entire shelf area emerged during the LGM. This long period of shelf emergence provided enough time and space for a complex channel system to develop, even in the vicinity of the shelf edge.

4.3 Circulation model of the SCS with comparison between modern and paleo circulation pattern

For a better understanding of differences in the regional oceanographic circulation system on the northern continental margin of the SCS, we carried out simulations with the 3D circulation model (explained in section 3.4) using the modern bathymetry (DEM_0) and reconstructed paleo-geographic bathymetries (paleo-$DEM_{60.5kyrBP}$ and paleo-$DEM_{65kyrBP}$, standing for MIS 3 SL high-stand and MIS 4 SL low-stand scenarios, respectively) and compare their results.

Results confirm that the patterns and variations of circulation of the SCS are largely driven by the East-Asian monsoon system (Liu et al., 2008). In typical modern winter conditions, current velocity (represented by vertically-averaged and seasonal mean values) is relatively high along the eastern coastline of the Hainan Island with values around 0.3-0.4 m/s and along the shelf break with values 0.4-0.5 m/s (Fig. 9a). Currents in the Beibu Gulf are relatively weak with values around 0.1-0.2 m/s along the western coastline and less than 0.1 m/s in the central part as well as along the western coastline of the Hainan Island. During summer, currents are energetic along both the south-western and north-eastern coastline of the Hainan Island with values around 0.2-0.3 m/s (Fig. 9b), while the rest part of the coastal area is characterized by relatively calm hydrodynamic conditions with current velocity generally below 0.1 m/s.

In the paleo-oceanographic scenarios, when the sea level mildly dropped from -48 m (MIS 3) to -56 m (R1: 56 kyr BP), the Beibu Gulf appeared as a coastal embayment and the Hainan Island was part of the South China mainland. During winter, energetic coastal currents (>0.3 m/s) occur along the eastern coastline of Hainan and Vietnam. Circulation in the embayment (Beibu Gulf) was characterized by a cyclonic gyre in winter (Fig. 9c) and anti-cyclonic gyre in summer (Fig. 9d), both with weak current velocity within 0.1 m/s.

In an earlier stage (MIS 4), as the sea level dropped and the coastline shifted seaward during glacial time (R2: 65 kyr BP), the embayment area was smaller and the shelf was narrower than in MIS 3. Simulation results show that in winter monsoon conditions, coastal currents along the south and south-eastern coastline of Hainan are quite strong, with velocity around 0.2-0.4 m/s (Fig. 9e). Alongshore coastal current with similar strength is also seen along a major part of the mainland coast. Such strong westward coastal currents would be able to efficiently transport sediment along its pathway (Zhang et al., 2020). Compared to the energetic hydrodynamic regime along the coast in winter, coastal currents in summer is much weaker and featured by velocity within 0.25 m/s (Fig. 9f).

5. Discussion

5.1 Paleogeographic evolution of the NW SCS

Based on the global SL change curve (Waelbroeck et al., 2002) and the DEM, we reconstructed paleogeographic shifts in the SCS, particularly its NW, in more detail (Figs 4 and 5), to provide a background for understanding sedimentary and oceanographic changes in the area.

During MIS 5, the warm climate induced rapid global SL rise, to values higher than today, so that Beibu Gulf was completely inundated. The SCS and Beibu Gulf were connected by surrounding ocean basins from the south and to the east (Figs 4a and 5a). The Vietnamese and Thai coastal plains and fluvial deltas were completely submerged, and the continental shelf expanded by > ~ 1 × 10^5 km^2. During MIS 4, in the NW SCS, Hainan Island was contiguous with the South China mainland, with the Qiongzhou Strait closed. At the MIS 4 SL minimum (65 kyr BP), climate cooling led to an SL drop, when, at its minimum, the area of Beibu Gulf was reduced by 70%, and it became transformed into a small embayment (Fig. 5b).

At this time, most SCS coastal areas, including Sunda Shelf and Beibu Gulf (Fig. 8a), were exposed, and subaqueous deltas developed in the NW SCS. Paleo-channels associated with these deltas transported sediment from the mainland to Beibu Gulf. Our modeling suggested that there was a strong coastal current along the S and SE Hainan Island coastline during winter monsoons, at that time, which could efficiently transport sediment along its path (Fig. 9e). Further morphodynamic simulation results showed that the sediments transported by the paleo-rivers along the SE Hainan Island coast facilitated formation of the Hainan delta, under the influence of this winter monsoon-driven circulation, astronomical tides, and buoyancy-driven river plumes (Zhang et al., 2020).

During the MIS 3 interglacial, Hainan Island was still connected with the south China mainland, even though the SL rose and the area of Beibu Gulf expanded. The Hainan delta continued to develop, until a termination in approximately 56 kyr BP. One hypothesis for its termination is that a change of the sediment routing system along the Hainan Island coast developed, resulting in a significant reduction of sediment supply for the delta. In a word, the DEM results revealed that Hainan Island may have been the main provenance contributor for the paleo-delta—and this was confirmed by evidence in the seismic profiles covering the study area.

5.2 Sediment transport in the NW SCS and Hainan delta formation during the LGC

Several rivers, including the Red, Ca, and Ma rivers in northern Vietnam, the Nanliu River in the south China mainland, and the Changhua Jiang, Ningyuan, and Louwang rivers on Hainan Island, flowed into Beibu Gulf (Milliman and Farnsworth, 2011; Yang et al., 2013). The modern sediment discharge rates of these rivers can be seen in Table 2, which shows that the Red River is the largest river in this region, with an annual sediment discharge of 110×10^9 kg (Milliman and Farnsworth, 2011; Yang et al., 2013). The Ca and Ma rivers were larger than local rivers in NW Hainan Island, transporting 4×10^9 and 3×10^9 kg / yr sediment to the Yinggehai Basin, respectively. In addition, the Nanliu River transported 0.032×10^9 kg / yr sediment from the south China mainland into the Yinggehai Basin.

The Changhua and Wanquan rivers are the two dominant rivers in south Hainan Island, contributing ~ 80% and ~ 85% of the sediment discharge from SW and SE Hainan Island, respectively. Meanwhile, the runoff and sediment discharge rates from major local Hainan rivers are relatively small today, compared to the Red River (Milliman and Farnsworth, 2011; Yang et al., 2013). Such sediment discharge rates (a total of ~ 1.8×10^6 t yr^{-1} from all major rivers in south Hainan in modern times), are too small to account for the previous average accumulation rate (~ 3×10^8 t yr^{-1}

between 65 and 56 kyr BP, Miluch et al., 2020) in the Hainan delta. Our morphodynamic modelling suggested that most sediments transported by the Red and Nanliu rivers in the NW SCS tended to deposit at their river mouths, with only small amounts being resuspended by typhoons and deposited into the Yinggehai Basin, contributing to the development of the Hainan delta (Zhang et al., 2020). Our simulation results also implied that there was at least ten-times more sediment being supplied from SW Hainan Island during the development of the river delta than takes place currently, with most of this accumulated in the Hainan delta.

The distribution of paleo-channels spotted on the subsurface of reflector R2 (65 kyr BP) during the MIS 4 SL minimum, and modelled from our seismic data and DEM data, showed that the channels on the Hainan Island SW shelf dipped down to the Yinggehai Basin, and served as sediment transport pathways (Fig. 8b). Directional semi-variograms from seismic interpretation were used to describe spatial variability by Miluch et al. (2020), and revealed that Sediment Unit (R0–R1), at 150°, and Sediment Unit (R1–R2), at 120°, have defined non-trending directions. They also identified sediment transport from the NE Hainan coast to the Yinggehai Basin, using the NW–SE prograding clinoforms, which marked the progradation of sediment sheets of similar thicknesses (Feng et al., 2018a). These results also supported our interpretation that Hainan Island served as the main source of delta sediment.

Evidence from detrital zircon U-Pb chronology, whole rock geochemistry, seismic datasets, and sediment flux analysis confirmed that the Red River played an important role in sediment transport in the NW SCS, whereas the effects of Hainan

Island and the Vietnamese margin were subordinate to this during the late Paleogene–early Neogene (Yan et al., 2011; Wang et al., 2014, 2016, 2019a, b; Cao et al., 2015; Zhao et al., 2015; Jonell et al., 2017). Cui et al. (2018) suggested that detrital zircon U-Pb chronologies and whole rock geochemistry revealed that the Red River, the central margin of Vietnam, and Hainan Island were the main Yinggehai Basin sediment sources. However, Hainan Island sediments were transported W into the central part of the Yinggehai Basin during the late Miocene–Pliocene, and Hainan Island was the primary source for upper Miocene–Pliocene sediments of the Qiongdongnan Basin. This suggested that the influence of Hainan Island sediments on the sedimentary evolution of the NW SCS during the late Miocene–Pliocene was greater than that of Red River or central Vietnam margin sediments.

It was also noted that the sedimentation rate between the formation of reflectors R2 and R1 rose from approximately 1 m / kyr to 5 m / kyr (Fig. 2), which led us to propose that intensified sediment supply outpaced SL rise during the MIS 4 / 3 transition, causing a normal regression (Kendall, 2016) and formation of the Hainan delta.

5.3 Factors controlling formation of the Hainan delta

Our results indicated that the Hainan delta developed during the MIS 4 / 3 transition, when the SL changed from a low SL (MIS 4) to high (MIS 3). The transition between MIS 4 and MIS 3 could be regarded as a “Failed Glacial Termination” (Cheng et al., 2016), and has been correlated with a relative SL rise resulting from increased Northern Hemisphere Summer Insolation and weak Asian monsoons. During the MIS 4 SL minimum period, various paleo-channels were incised, which delivered the sediment mass from Hainan Island to the Yinggehai Basin. As discussed above, sediment supply outpaced SL rise during the MIS 4 / 3 transition, causing normal regression and formation of the Hainan delta—suggesting that the SL rise and a remarkable increase in sediment supply were the factors controlling Hainan delta formation.

In considering why a sediment mass was transported to the basin, we noted that there was a high sediment accumulation rate during the delta formation period (~ 5 m / kyr compared to ~ 1 m / kyr before and after delta accumulation). This could have been caused theoretically by tectonic uplift and intensified erosion from land surfaces, and by regional changes to monsoon patterns, all of which would result in increased coastal erosion. The balance between Hainan Island uplift and Beibu Gulf subsidence (including the Yinggehai Basin) should be considered when evaluating the role of tectonics. The subsidence rate of the central Yinggehai Basin was ~ 4 mm / yr (Lin et al., 1997), although this process was not linearly declining after the accumulation of Neogene sediments.

We considered the sediment contribution from MIS 4 to the present-day, which has been ~ 0.1 mm / yr (Groh and Harff, 2020). The tectonic uplift of Hainan Island in particular, with respect to the mantle plume hypothesis, has been discussed intensely in the literature (Xia et al., 2016). A set of vertical crustal movement data was published by Hu et al. (2015), although these data only referenced a fixed point on Hainan Island, and were not integrated into a supra-regional geodetic network of reference points. To estimate the uplift dimensions, we compared the present position of AMS- and OSL-dated samples from SW Hainan Island with paleo-height estimates in the SL curve of Waelbroeck et al. (2002), which allowed us to estimate uplift rates between 1 and 2 mm / yr for the LGC. These data agreed with most studies published about the vertical crustal movement of Hainan Island, even though our assumption was based on dating just two samples (Borowka et al., 2020).

Mestdagh et al. (2019) discussed factors controlling the stratigraphic architecture of the northern Gulf of Cadiz during the Quaternary, and suggested that: (1) seismic stratigraphic elements and tectonics mainly controlled the seismic stacking patterns on timescales of several hundreds of kyr; (2) SL played a critical role in all seismic stratigraphic elements on timescales ≤ ~ 100 kyr; and (3) on similar timescales, oceanography mostly influences depocenter distribution, internal architecture, and seismic facies. Considering this issue, we determined that it was unlikely that a sudden increase of tectonic uplift between 65 and 56 kyr BP caused surface erosion sufficient to provide the sediment source for the Hainan delta. The assumption that external (meteorological) forces played a role in the anomalies of sediment supply for Hainan delta accumulation sounded more plausible.

Tomczak et al. (2020) reconstructed sea surface temperatures (SST) for the time span from 65 to 56 kyr BP, the formation time of the Hainan delta, using biomarker proxy-data analyses of ZBW core samples. According to their SST reconstruction, the paleo-temperature dropped at 65 kyr BP before returning to warmer conditions at 61 kyr BP, but at no stage did it reach the relatively higher MIS values. The temperature drop at 65 kyr BP coincided with a positive anomaly in the $\delta^{18}O$ record, supporting the hypothesis of a weakened Asian Summer Monsoon at this time; this weakened monsoon resulted in lower temperatures and precipitation, which counters the concept of a high supply of erosional products by riverine transport.

We have reviewed meteorological reanalysis data (Compo et al., 2011) covering the period 1871–2012, from the 20CR v2 project, to test whether greater monsoon intensity was also connected with higher precipitation in the Hainan region. Meteorological reanalysis is the product of a numerical weather prediction model that is nudged towards available observations, producing an optimal blending of observations and modelled atmospheric dynamics. In this reanalysis data set, we noted that Hainan Island precipitation correlated negatively with precipitation over much of the rest of monsoon-affected Asia, which indicated that strengthened winter monsoon conditions in Asia did not exclude very high rainfall rates at Hainan Island (Fig. 10).

We also noted that winters in this period, with higher average precipitation, also tended to witness extremes of strong daily precipitation—and these conditions might also have happened during formation of the Hainan delta. Our hypothesis was supported by paleo-oceanographic modeling based on paleogeographic scenarios for paleo-$DEM_{56kyrBP}$ and paleo-$DEM_{65kyrBP}$ (Fig. 7), and on Beibu Gulf paleo-circulation models, which included effects from major rivers, and tides, and extreme events such as typhoons (Zhang et al., 2020).

Zhang et al. (2020) modeled morphological development of the Hainan delta over 50 y, to investigate sediment transport and sedimentation processes associated with formation of the paleo-delta. They found that comparison of summer and winter monsoon conditions showed that delta formation developed from the combined effects of two distinct seasonal monsoons, and their interactions with buoyancy-driven river plumes and astronomical tides. The contribution of the Red River to delta development was less than that of local rivers in SW Hainan, due to the combined effects of regional circulation and tides, which caused the buoyancy-driven plume to detour around the delta, despite having greater runoff and sediment discharge rates compared to those from local Hainan rivers. The simulated bed level changes were consistent with the morphology of the Hainan delta, suggesting that both climate (as represented by SL) and oceanography were important preconditions for Hainan delta genesis. We also concluded that intensified longshore transport from the eastern Hainan coast, which was part of the mainland during the SL minimum, might have also supplied sediment for delta development.

6. Conclusions

(1) During MIS 5, the warm climate induced rapid global SL rise, to levels higher than those seen today, which submerged Beibu Gulf completely. The SCS and Beibu Gulf were connected with its surrounding marine basins by gateways and straits to the east and to the south, respectively. The climate cooled during MIS 4, so that Beibu Gulf partly re-emerged during the relatively low SL. On the appearance of alluvial plains, rivers produced incised valleys which delivered sediment to the river mouths, forming depositional systems such as deltas. During MIS 3, the rising SL level resulted in the submergence of the SCS shelves, including Sunda Shelf and Beibu

Gulf, and the shoreline retreated by more than half of the width of the modern continental shelf. During the LGM, the SL dropped rapidly, to ~ 123 m lower than the present-day, during MIS 2. A major part of the SCS continental shelf emerged, and reverted to a terrestrial environment.

(2) The results of the study described here supported the hypothesis that Hainan delta sediments formed between 65 and 56 kyr BP, and consisted mainly of weathering products from Hainan Island. Intensified sediment supply outpaced SL rise at the MIS 4 / 3 transition, causing a “normal regression” effect. Intensified land-surface and coastal erosion, which were the results of changing regional monsoon activity, caused high levels of sediment supply, which led to accretion at the rate of ~ 5 m / kyr, compared to ~ 1 m / kyr before and after delta accumulation. We considered that the shift of the Asian Monsoon system to a stronger winter monsoon, connected with local meteorological effects on Hainan Island and global SL changes, were the main drivers controlling sediment source-to-sink systems during the LGC at the northern continental margin of the SCS.

Acknowledgements

This work is funded by the Polish National Center of Science (NCN), Research Project “Evolution of the Hainan delta (SCS’s northwestern shelf) as a response to changes in paleoenvironment since Late Pleistocene”(NCN-ID: 2016/21/B/ST10/02939 US-ID: 505-1100-250837) and the China Geological Survey Projects (No.GZH201500207, DD20160138 and No.DD20160146). The authors are grateful to the China University of Geosciences (Wuhan), University of Szczecin

(Poland) and the Helmholtz –Zentrum Geesthacht (Germany) for their support and effort to my aboard study as a visiting PHD student. Thanks to Guangzhou Marine Geological Survey (China) and Leibniz Institute for Baltic Sea Research (Germany) for the cooperation.

References

Allen, P.A., Allen, J. R., 2008. Basin Analysis – Priciples and Applications. Blackwell Publishing, Oxford, pp. 1 – 549.

Allen, C.R., Gillespie, A.R., Han, Y., Sieh, K.E., Zhang, B., Zhu, C., 1984. Red River and associated faults in Yunnan Province, China: quaternary geology, slip rates and seismic hazard. Geol. Soc. Amer. Bull 95, 686–700. doi：10.1130/0016-7606(1984)95<686:RRAAFY>2.0.CO;2

Blumberg, A.F., Mellor, G.L., 1987. A description of a three-dimensional coastal ocean circulation model. In: Heaps, N.S. (Ed.), Three-Dimensional Coastal Ocean Models. American Geophysical Union, Washington, DC, pp. 1–16.

Borówka, R.K., Maciąg, Ł., Osadczuk, A., Jiang, T., Chen, H., Osadczuk, K., Miluch, J., Harff, J., Tomkowiak, J., Bloom, K., and Li Ch. Best regards, Lukasz Maciag. Pleniglacial to Late Pleistocene evolution of the lower segments of river valleys in the southwestern Hainan Island, South China Sea. Journal of Asian Earth Science 195 (2020, forthcoming).

Bresnahan, T., Dickenson, K., 2002. Surfer 8 self-paced training guide. Golden Software Inc.

Briais, A., P. Patriat, and P. Tapponnier., 1993. Updated interpretation of magnetic anomalies and seafloor spreading in the South China Sea: Implications for the tertiary tectonics of Southeast Asia. Journal of Geophysical Research 98, 6299–6328. doi：10.1029/92JB02280

Caruso, M.J., Gawarkiewicz, G.G., Beardsley, R.C., 2006. Interannual variability of the Kuroshio intrusion in the South China Sea. Journal of Oceanography 62, 559–575. doi：10.1007/s10872-006-0076-0

Chen, H., Harff, J., Qiu, Y., Osadczuk, A., Zhang, J., Tomczak, M., Cui, Z., Cai, G., 2016. Last Glacial Cycle and Seismic Stratigraphical Sequences at the West Offshore of Hainan Island, Northwestern of the South China Sea. In: Clift, P. D., Harff, J., Wu, J., Qiu, Y. (eds) River-Dominated Shelf Sediments of East Asian Seas. Geological Society, London, Special Publications, 429, http://doi.org/10.1144/SP429.

Chen, H., Xie, X., Zhang, W., Shu, Y., Wang, D., Vandorpe, T., Van Rooij, D., 2016. Deepwater sedimentary systems and their relationship with bottom currents at the intersection of Xisha Trough and Northwest Sub-Basin, South China Sea. Marine Geology 378, 101–113.

Chen, H., Zhang, W., Xie, X., Ren, J., 2019. Sediment dynamics driven by contour currents and mesoscale eddies along continental slope: A case study of the northern South China Sea. Marine Geology 409, 48-66.

Cheng, H., Edwards, R. L., Sinha, A., Spotl, C., Yi, L., Chen, S., Kelly, M., Kathayat, G., Wang, X. F., Li, X. L., Kong, X. G., Wang, Y. J., N, Y. F., Zhang, H. W., 2016.

The Asian monsoon over the past 640,000 years and ice age terminations. Nature, 534, 640. 10.1038/nature18591

Dansgaard, W., S.J. Johnsen, S.J., Clausen, H.B., Dahl-Jensen, D., Gundestrup, N.S., Hammer, C.U., Hvidberg, C.S., Steffensen, J.P., Sveinbjornsdottir, A.E., Jouzel, J., Bond, G., 1993. Evidence for general instability of past climate form a 250-kyr ice-core record. Nature 364, 218–220. doi:10.1038/364218a0

Deng, J., Harff, J., Zhang, W., Schneider, R., Durzinska-Nowak, J., Giza, A., Terefenko, P., and Furmanczyk, K., 2017. The Dynamic Equilibrium Shore Model for the Reconstruction and Future Projection of Coastal Morphodynamics. In: Harff J, Furmanczyk K, von Storch H (eds) Coastline changes of the Baltic Sea from south to east – past and future projection. Coastal research library, vol 19. Springer, Cham, Switzerland. DOI:10.1007/978-3-319-49894-2

Egbert, G. D., and L. Erofeeva., 2002. Efficient inverse modeling of barotropic ocean tides. Journal of Atmospheric and Oceanic Technology 19, 183–204. doi:10.1175/1520-0426(2002)019<0183:eimobo>2.0.co;2

Mestdagh, T., Lobo, F. J., Estefanía Llave., F. Javier Hernández-Molina, & Rooij, D. V., 2019, Review of the late quaternary stratigraphy of the northern gulf of cadiz continental margin: new insights into controlling factors and global implications. 198, 102944. https://doi.org/10.1016/j.earscirev.2019.102944

Gao, J., H. Xue, F. Chai, and M. Shi, 2013, Modeling the circulation in the Gulf of Tonkin, South China Sea. Ocean Dynamics 63, 979–993. doi: 10.1007/s10236-013-0636-y.

Fang, G.H., Fang, W.D., Fang, Y., Wang, K., 1998. A survey of studies on the South China Sea upper ocean circulation. Acta Oceanogr. Taiwan 1, 1–16.

Fang, G., Kwok, Y.K., Yu, K., Zhu, Y., 1999. Numerical simulation of principal tidal constituents in the South China Sea, Gulf of Tonkin and Gulf of Thailand. Continental Shelf Research 19, 845-869.

Feng, Y. C., Zhang, W. H., Cheng, H. J., Jiang, T., Zhang, J. C., Osadczuk, A., Yao, Y. T., Li, W., Sun, J., Guo, L., Huang, W. K., Li, S., Zhang, W. Y., 2018a. Seismic characteristics and sedimentary record of the late Pleistocene delta offshore south-western Hainan Island, north-western South China Sea. Interpretation, 6, 31-43.

Feng, Y. C., 2018b. Paleo-geomorphology evolution and controlling factors of the late Pleistocene delta offshore south-western Hainan Island, north-western South China Sea. Doctor Thesis, 38.

Groh, A., Harff, J., 2020, (forthcoming). Modelling relative sea-level changes induced by water and sediment loads in the Beibu Gulf, South China Sea. Journal of Asian Earth Sciences 195 (2020, forthcoming)

Hanebuth, T., Saitob, Y., Tanabe, S., Vuc, Q. L., Ngo, Q., T., 2006. Sea levels during late marine isotope stage 3 reported from the Red River delta (northern Vietnam) and adjacent regions. Quaternary International 145–146, 119–134.

Hanebuth, T.J.J., K. Stattegger, A. Bojanowski, 2009: Termination of the Last Glacial Maximum sea-level lowstand: The Sunda-Shelf data revisited. Global and Planetary Change 66, 76–84.

Hanebuth, T.J.J., Stattegger K. Schimanski A., Lüdmann T., How Kin Wong, 2003: Late Pleistocene force dregressive deposits on the Sunda Shelf (Southeast Asia). Marine Geology 199, 139-157.

Hanebuth, T.J.J., Voris H.K., Yokoyama Y., 2011: Formation and fate of sedimentary depocentres on Southeast Asia's Sunda Shelf over the past sea-level cycle and biogeographic implications. Earth-Science Reviews 104, 92-110.

Hanebuth, T.J.J., Zhang, W., Hofmann, A.L., Löwemark, L.A., Schwenk, T., 2015. Oceanic density fronts steering bottom-current induced sedimentation deduced from a 50 ka contourite-drift record and numerical modeling (off NW Spain). Quaternary Science Reviews 112, 207–225.

Haq, B. U., Hardenbol, J., Vail, P. R., 1987: The chronology of fluctuating sea levels since the Triassic. Science 235, 1156-1167.

Harff, J., Flemming, N., Groh, A., Hünicke, B., Lericolais, G., Meschede, M., Rosentau, A., D. Sakellariou, D., Uscinowicz, S., Zhang, W., Zorita, E., 2014, in print: Sea level and climate. in: Flemming, N., Harff, J., Moura, D. (eds.): Quaternary paleoenvironments. Dordrecht: Blackwell: 1-54.

Harff, J., Leipe, T., Waniek, J., Zhou, Di. (eds.), 2013: Depositional Environments and Multiple Forcing Factors at the South China Sea's Northern Shelf, Journal of Coastal Research: SI 66, 90 p.

Harff, J., Meyer, M., 2011: Coastlines of the Baltic Sea - zones of competition between geological processes and a changing climate: Examples from the southern Baltic.- in: Harff, J., Björck, S., Hoth, P. (eds,) 011: The Baltic Sea

Basin.- Springer: Berlin et al., p. 149-164.

Harff, J., Meyer, M., Zhang, W., Barthel, A., Naumann, M., 2011: Holocene sediment dynamics at the southern Baltic Sea. Berichte der Römisch-Germanischen Kommission, 92: 41-76.

Harff, J.; Lemke, W.; Lampe, R.; Lüth, F.; Lübke, R.; Meyer, M.; Tauber, F.; Schmölcke, U., 2007: The Baltic Sea Coast - a Model of Interrelations between Geosphere, Climate and Anthroposphere. In: Harff, 6 J.; Hay, W.W.; Tetzlaff, D. (eds.): Coastline Change – Interrelation of Climate and Geological Processes. The Geological Society of America, Spec. Pap. 426: 133-142.

Harff. J., Waniek, J., Xia, Z., (eds.), 2009: Cruise Report R/V FENDOU-5 September 23 to October 16, 2009 from Guangzhou to Guangzhou. Unpubl. Report, Guangzhou Marine Geological Survey, Leibniz-Institute for Baltic Sea Research Warnemünde, Guangzhou, October 16, 2009, 35 p., 6 encl.

Hu, J., Kawamura, H., Hong, H., Qi, Y., 2000. A review on the currents in the South China Sea: seasonal circulation, South China Sea warm current and Kuroshio intrusion. Journal of Oceanography 56, 607–624.

Huang W., Chen H., Qiu Y., 2015: Seismic stratigraphic features of the late Pleistocene delta of the Yinggehai Basin, northwest of South China Sea. Marine Geology Frontiers 8,10-15

Kendall, C.G., 2016. Sedimentary Sequence. in: Harff, J., Meschede, M., Peterson, S., Thiede, J. Encyclopedia of Marine Geosciences. Springer, New York, 768 – 773.

Krone, R.B., 1962. Flume studies of the transport of sediment in estuarial shoaling processes. Hydraulic Engineering Laboratory and Sanitary Engineering Research Laboratory, University of California, Berkeley.

Lee, C., Schwab, D.J., Hawley, N., 2005. Sensitivity analysis of sediment resuspension parameters in coastal area of southern Lake Michigan. Journal of Geophysical Research 110, C03004.

Lericolais G, Bulois C, Gillet H, Guichard F., 2009: High frequency sea level fluctuations recorded in the Black Sea since the LGM[J]. Global and Planetary Change 66, 65-75.

Leloup, P.H., Lacassin, R., Tapponnier, P., Schärer, U., Zhong, D., Liu, X., Zhang, L., Ji, S., Trinh, P.T., 1995. The Ailao Shan-Red River shear zone (Yunnan, China), Tertiary transform boundary of Indochina. Tectonophysics 251, 3–84.

Liu, Q., A. Kaneko, and J. Su, 2008, Recent progress in studies of the South China Sea circulation: Journal of Oceanography, 64, 753–762, doi: 10.1007/s10872-008- 0063-8.

Liu, Z., Zhao, Y., Colin, C., Stattegger, K., Wiesner, M.G., Chih-An Huh., Zhang, Y., Li, X., Sompongchaiyakul, P., Chen-Feng You., Chi-Yue Huang., Liu, J.T.., Siringan, F.P., Khanh Phon Le., Sathiamurthy, E., Hantoro, W.S., Liu, J., Tuo, S., Zhao, S., Zhou, S., He, Z., Wang, Y., Bunsomboonsakul, S., Li, Y., 2016. Source-to-sink transport processes of fluvial sediments in the South China Sea. Earth-Science Reviews 153, 238-273.

Lu, W., C. Ke, J. Wu, J. Liu, and C. Lin., 1987. Characteristics of magnetic lineations and tectonic evolution of the South China Sea basin, Acta Oceanogr. Sin., 6, 577–588.

Lobo, F, Ridente, D., 2013. Stratigraphic architecture and spatio-temporal variability of high-frequency Milankovitch depositional cycles on modern continental margins: An overview. Marine Geology 52,2015-247.

Mccalpin, J.D., 1994. A comparison of second-order and fourth-order pressure gradient algorithms in a σ-co-ordinate ocean model. Int. J. Numer. Methods Fluids 18, 361–383.

McCave, I.N. and Swift, S.A., 1976. A physical model for the rate of deposition of fine-grained sediments in the deep sea. Geological Society of America Bulletin 87, 541-546.

Mellor, G.L., 2003. Users Guide for a Three-Dimensional, Primitive Equation, Numerical Ocean Model. Atmospheric and Oceanic Sciences Princeton University.

Milankovitch, M., 1930. Matematische Klimalehre und astronomische Theorie der Klimaschwankungen. In: Köppen, W., Geiger, R. (Eds.), Handbuch der Klimatologie, I (A). Gebrüder Borntraeger, Berlin, pp. 1–176.

Milankovitch, M., 1941. Kanon der Erdbestrahlung und seine Anwendung auf das Eiszeitproblem. Akademie Royale Serbe 133, 1–633.

Milliman J D, Farnsworth K L. River discharge to the coastal ocean[M]// River discharge to the coastal ocean: a global synthesis. 2011.

Miluch, J., Osadczuk A., Chen H., Feldens P., Harff J., Maciąg Ł., 2020 (forthcoming). Seismic profiling-based investigation of geometry and sedimentary architecture of the late Pleistocene delta in the Beibu Gulf, SW of Hainan Island. Journal of Asian Earth Sciences 195 (2020, forthcoming)

Mitchum, R.M.J., Van Wagoner, J.C., 1991. High-frequency sequences and their stacking patterns: sequence-stratigraphic evidence of high-frequency eustatic cycles. Sedimentary Geology 70, 131–160

Molnar P, Tapponnier P, 1975. Cenozoic Tectonics of Asia: Effects of a Continental Collision: Features of recent continental tectonics in Asia can be interpreted as results of the India-Eurasia collision. Science 4201, 419-426.

Nagashima, K., Tada, R., Matsui, H., Irino, T., Tani, A., Toyoda, S., 2007. Orbital- and millennial-scale variations in Asian dust transport path to the Japan Sea. Palaeogeography, Palaeoclimatology, Palaeoecology 247, 144–161.

Ni, Y., Endler, R., Xia, Z., Endler, M., Harff, J., Gan, H., Schulz-Bull, D. E., Waniek, J. J., 2014. The “butterfly delta” system of Qiongzhou Strait. morphology, seismic stratigraphy and sedimentation. Marine Geology 355, 361-368.

Ni, Y., Harff, J., Xia, Z., Waniek, J. J., Endler, M., Schulz-Bull, D. E., 2016. Post-glacial mud depocentre in the southern Beibu Gulf. acoustic features and implication for the sedimentary environment evolution. in. Clift, P. D., Harff, J., Wu,J., Yan, Q. (eds.). River-Dominated Shelf Sediments of East Asian Seas. Geological Society, London, Special Publications 429, 87-98.

Olea RA, 1999. Geostatistics for Engineers and Earth Scientists. Kluwer Academic Publishers, Boston

Oliver, M. A., & Webster, R., 1990. Kriging: a method of interpolation for geographical information systems. International Journal of Geographical Information System 4, 313-332.

Oliver, M. A., & Webster, R., 2014. A tutorial guide to geostatistics: Computing and modelling variograms and kriging. Catena 113, 56-69.

Pairaud, I.L., Auclair, F., Marsaleix, P., Lyard, F., Pichon, A., 2010. Dynamics of the semi-diurnal and quarter-diurnal internal tides in the Bay of Biscay. Part 2: Baroclinic tides. Continental Shelf Research 30 253-269.

Peltier, W.R., 2004. Global glacial isostasy and the surface of the ice-age Earth: The ICE-5G(VM2) model and GRACE. Annu. Rev. Earth Planet. Sci. 32, p. 111-149.

Peter D. Clift, Zhen Sun, 2006. The sedimentary and tectonic evolution of the Yinggehai–Song Hong basin and the southern Hainan margin, South China Sea: Implications for Tibetan uplift and monsoon intensification. Journal of Geophysical Research: Solid Earth 111.

Pubellier, M., Savva, D., Aurelio, M., Sapin, F., 2016. Structural Map of the South China Sea / Commission for the Geological Map of the World. UNESCOSchulz-Bull. D., Waniek, J. (eds.), 2011: RV SONNE CRUISE SO219, 01.12.-24.12.2011 Manila - Hong Kong, Leibniz-Institute for Baltic Sea Research Warnemünde, 40 p., 5 encl.

Qu, T.D., Girton, J.B., Whitehead, J.A., 2006. Deepwater overflow through Luzon Strait. J. Geophys. Res. 111, C01002. http://dx.doi.org/10.1029/2005JC003139.

Rangin C, Silver E A, Tamaki K, 1995. Closure of western Pacific marginal basins: Rupture of the oceanic crust and the emplacement of ophiolites. Geophysical

Monograph Series 88, 405-417. DOI: 10.1029/GM088p0405
Rea, D.K., Hovan, S.A., 1995. Grain size distribution and depositional processes of the mineral component of abyssal sediments: Lessons from the North Pacific. Paleoceanography 10, 251–258.
Schulz-Bull, D., Waniek, J, Plewe, S. et al., 2012. RV SONNE cruise SO219 - 01.12.-24.12.2011 - Manila - Hong Kong - Holocene environmental evolution and anthropogenic impact of Beibu Gulf, South China Sea. Leibniz-Institut for Baltic Sea Research, Warnemünde, 99 p.
Simmons, H., Chang, M. H., Chang, Y. T., Chao, S. Y., Fringer, O., Jackson, C.R., Ko, D.S., 2011. Modeling and prediction of internal waves in the South China Sea. Oceanography 24, 88-99.
Shi, X., Kohn, B., Spencer, S., Guo, X., Li, Y., Yang, X., Shi, H., Gleadow, A., 2011. Cenozoic denudation history of southern Hainan Island, South China Sea: Constraints from low temperature thermochronology. Tectonophysics 504, 100-115.
Sathiamurthy, E., Voris, H.K., 2006. Maps of Holocene sea level transgression and submerged lakes on the Sunda Shelf. The Natural History Journal of Chulalongkorn University, Supplement 2, 1–43.
Shu, Y., Xue, H., Wang, D., Chai, F., Xie, Q., Yao, J., and Xiao, J., 2014. Meridional overturning circulation in the South China Sea envisioned from the high-resolution global reanalysis data GLBa0.08. Journal of Geophysical Research Oceans 119, 3012–3028.

Sun Z, Zhou D, Zhong Z, Zeng, Z. X., Wu, S. M., 2003. Experimental evidence for the dynamics of the formation of the Yinggehai Basin, NW South China Sea. Tectonophysics 1, 41-58.

Sun, W.W., Shen, J., Yu, S.Y., Long, H., Zhang, E. L., Liu, E. F., Chen, R., 2018. A lacustrine record of East Asian summer monsoon and atmospheric dust loading since the last interglaciation from Lake Xingkai, northeast China. Quaternary Research 89, 270-280. 10.1017/qua.2017.81

Spratt, R. M., Lisiecki, L. E. A., 2015. Late Pleistocene sea level stack. Clim.Past Discuss.: 11, 3699-3728.

Steffensen, J.P., 1997. The size distribution of microparticles from selected segments of the Greenland Ice Core Project ice core representing different climatic periods. Journal of Geophysical Research: Oceans 102, 26755–26763

Tanabe, S., Saito, Y., Quang, L. V., Till, J. J., Hanebuth., Quang, L. N., Akihisa, K., 2006. Holocene evolution of the Song Homg (Red River) delta System, north Vietnam. Sedimentary Geology 187: 29-61.

Tapponnier, P., G. Peltzer, and R. Armijo, 1986. On the mechanics of the collision between India and Asia, in Collision Tectonics, edited by M. P. Coward and A. C. Ries, Geol. Soc. Spec. Publ., 19, 115–157.

Tangang, F.T., Xia, C.S., Qiao, F.L., Juneng, L., Shan, F., 2011. Seasonal circulation in the Malay Peninsula eastern continental shelf from a wave-tide-circulation coupled model. Ocean Dynamics 61, 1317–1328.

Taylor, B., and Hayes, D. E., 1980. The tectonic evolution of the south China basin, in

The Tectonic and Geologic Evolution of Southeast Asian Seas and Islands, Geophys. Monogr. Ser., vol. 23, edited by D. E. Hayes, pp. 89– 104, AGU, Washington, D. C.

Tomczak, M., Kaiser, J., Zhang, Voss, M., Huang, W. Hang, W., Arz, H., Harff, J., 2020 (forthcoming). Sea level and monsoon effects on terrigenous inputs and temperature in the northern-western South China Sea (Hainan Island) during the last glacial. (2020, forthcoming).

Tian, J. and Qu, T., 2012. Advances in research on the deep South China Sea circulation. Chinese Science Bulletin 57, 3115-3120.

Vail, P. R., Audemard, F., Bowman, S. A., Eisner, P. N., Perez-Cruz, C., 1991. The stratigraphic signatures of tectonics, eustasy and sedimentology an overview. in: Einsele, G., Ricken, W., Seilacher, A. (eds.), 1991: Cycles and Events in Stratigraphy.- Springer: Berlin et al., p. 617-659.

Van Rijn, L.C., 2007. Unified view of sediment transport by currents and waves, I: Initiation of motion, bed roughness, and bed-load transport. Journal of Hydraulic Engineering 133, 649-667.

Van Wagoner Je, Mitchum R.M., Campion K.M., Rahmanian V.D., 1990. Siliciclastic Sequence Stratigraphy in We ll Logs, Cores, and Outcrops: Concepts fo r High-Resolution Correlation of TIme and Fa cies. Am. Assoc. Petrol. Geol. Methods in Exploration Series, No.7. 55 pp.

Van Wagoner J.C., Posamentier H.W., Mitchum R.M. Jr, Vail P.R., Sarg J.F., et al., 1988. An overview of the fundamentals of sequence stratigraphy and key definitions. In: Wilgus, C. K., Hastings, B. S., Posamentier, H. et al. (eds.) 1988. Sea-Level Changes – An Integrated Approach. Society of Economic Paleontologists and Mineralogists, Special Publication No. 42, pp. 39-45.

Waelbroeck, C., Labeyrie, L., Michel, E., Duplessy, J.C., McManus, J.F., Lambeck, K., Balbon, E., Labracherie, M., 2002. Sea- level and deep water temperature changes derived from benthic foraminifera isotopic record, Quaternary Science Reviews 2, 295–305.

Wattayakorn, G., King, B., Wolanski, E., Suthanaruk, P., 1998. Seasonal dispersion of petroleum contaminants in the Gulf of Thailand. Cont. Shelf Res. 641–659.

Wang, G.H., Xie, S.-P., Qu, T.D., Huang, R.X., 2011. Deep South China Sea circulation. Geophys. Res. Lett. 38, L05601. http://dx.doi.org/10.1029/2010GL046626.

Webster, P.J., 1994. The role of hydrological processes in ocean–atmosphere interactions. Rev. Geophys. 32, 427–476.

Wu, D.X., Wang, Y., Lin, X.P., Yang, J.Y., 2008. On the mechanism of the cyclonic circulation in the Gulf of Tonkin in the summer. J. Geophys. Res. 113, C09029. http://dx.doi.org/ 10.1029/2007JC004208.

Wyrtki, K., 1961. Physical oceanography of the Southeast Asian waters. NAGA Report vol 2. University of California, Scripps Institution of Oceanography, La Jolla, California, pp. 1–195.

Wong, W. S. D., Lee, J., 2005. Statistical analysis of geographic information with ArcView GIS and ArcGIS. Wiley.

Xia, H.Y., Li, X.H., Shi, M.C., 2001. Three-D numerical simulation of wind-driven current and density current in the Beibu Gulf. Acta Oceanological Sinica 4, 455–472.

Xia, S., Zhao, D., Sun, J., Huang, H., 2016. Teleseismic imaging of the mantle beneath southernmost China: New insights into the Hainan plume. Gondwana Research 36, 45-56. doi: 10.1016/j.gr.2016.05.003

Xie, X., Müller R.D., Ren, J., Jiang, T., Zhang, C., 2008. Stratigraphic architecture and evolution of the continental slope system in offshore Hainan, northern South China Sea. Marine Geology. 247, 129-144.

Yan Y, Carter A, Palk C, Stephanie, B., Hu, X., 2013. Understanding sedimentation in the Song Hong–Yinggehai Basin, South China Sea. Geochemistry Geophysics Geosystems 12, 1-15. 10.1029/2011GC003533

Yang, C. S., Kao, S. P., Lee, F. B., Hung, P. S., 2004. Twelve different interpolation methods: A case study of Surfer 8.0, Proceedings of the XXth ISPRS Congress 35, 778-785.

Yao, Y., Harff, J., Meyer, M., Zhan, W., 2009. Reconstruction of paleocoastlines for the northwestern South China Sea since the Last Glacial Maximum. Science in China Series D: Earth Sciences, 52(8): 1127-1136.

Yin, S., Hernández-Molina, F.J., Zhang, W., Li, J., Wang, L., Ding, W., and Ding, W., 2019. The influence of oceanographic processes on contourite features: A multidisciplinary study of the northern South China Sea. Marine Geology 415, doi:10.1016/j.margeo.2019.105967

Zhang, W., Harff. J and Schneider, R., 2011. Analysis of 50-year wind data of the southern Baltic Sea for modelling coastal morphological evolution - a case study from the Darss-Zingst Peninsula. Oceanologia, 53 (1-TI), 489-518. doi:10.5697/oc.53-1-TI.489

Zhang, W., Harff, J., Schneider, R., Meyer, M., Zorita, E., Hünicke, B., 2014. Holocene morphogenesis at the southern Baltic Sea: simulation of multiscale processes and their interactions for the Darss-Zingst peninsula. Journal of Marine Systems 129, 4-18. doi:10.1016/j.jmarsys.2013.06.003

Zhang, W., Hanebuth, T.J.J., Stöber, U., 2016a. Short-term sediment dynamics on a mesoscale contourite drift (off NW Iberia): impacts of multi-scale oceanographic processes deduced from the analysis of mooring data and numerical modelling. Mar. Geol. 378, 81–100.

Zhang, W., Cui, Y., Santos, A.I., Hanebuth, T.J.J., 2016b. Storm-driven bottom sediment transport on a high-energy narrow shelf (NW Iberia) and development of mud depocenters. J. Geophys. Res. Oceans 121, 5751–5772.

Zhang, W., Xiong, P., Meng, Q., Dudzinska-Nowak, J., Chen, H., Zhang, H., Zhou, F., Harff, J. 2020. Morphogenesis of a late Pleistocene delta off the south-western Hainan Island unraveled by numerical modeling. Journal of Asian Earth Sciences, 195, 104351.

Zhao M. X., Huang C. Y., Wang C. C., Wei, G. J., 2006. A millennial-scale U 37 K′, sea-surface temperature record from the South China Sea (8°N) over the last 150kyr: Monsoon and sea-level influence. Palaeogeography Palaeoclimatology

Palaeoecology 1, 39-55.

Zhao, W., Zhou, C., Tian, J.W., Yang, Q.X., Wang, B., Xie, L.L., Qu, T.D., 2014. Deep water circulation in the Luzon Strait. J. Geophys. Res. Oceans 119, 790–804. http://dx.doi. org/10.1002/2013JC009587.

Guo, L. Z., Zhong, Z. H., Wang, L. S., Shi, Y. S., Li, H., Liu, S. W., 2001. Regional Tectonic Evolution Around Yinggehai Basin of South China Sea. Acta Metallurgica Sinica, 7, 1-12.

Zu, T., Gan, HP., Erofeeva, S.Y., 2008. Numerical study of the tide and tidal dynamics in the South China Sea. Deep Sea Research. Part I: Oceanographic Research Papers, 55, 137-154. http://dx.doi. 10.1016/j.dsr.2007.10.007

Table

Table.1 Selected global sea-level data (modified from Waelbroeck et al., 2002)

Table.2 Hydrological characteristics of today's rivers surrounding Beibu Gulf (Milliman and Farnsworth, 2011; Yang et al., 2013）

Figures

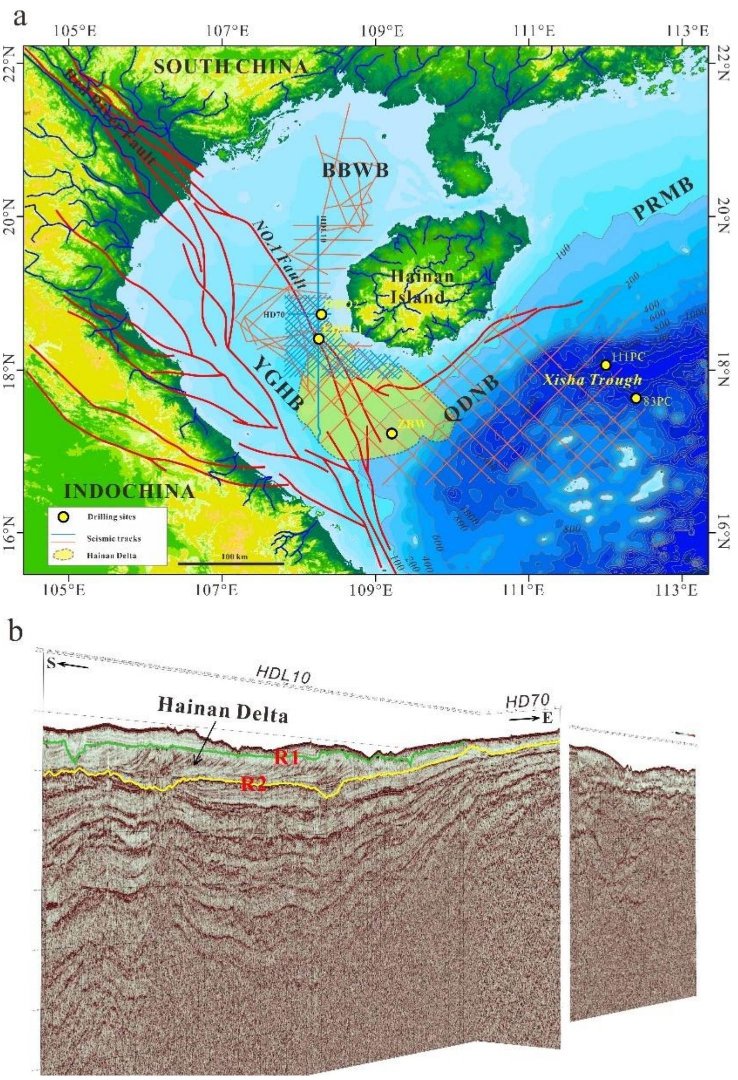

Figure 1. (a) DEM of the Beibu Gulf and adjacent terrestrial areas showing the bathymetry and location of the Beibu Gulf, with the location of 1) the profiles in Fig.1b and 2) the ZBW core. Seismic data used in our study are shown as blue and orange track plots. Sites of sediment cores ZBW, HDQ2, and LWD-1 are depicted by yellow spots. The yellow shaded area represents the Hainan delta. DEM data source is the GEBCO_2014 Grid, version 20150318, http://www.gebco.net. (b) Seismic N-S profile HDL10, crossing W-E profile HD70, and the characteristics of seismic reflectors R1 (green line) and R2 (yellow line) in the Yinggehai Basin. BBWB, Beibuwan Basin; YGHB, Yinggehai Basin; QDNB, Qiongdongnan Basin; PRMB,

Pear River Mouth Basin.

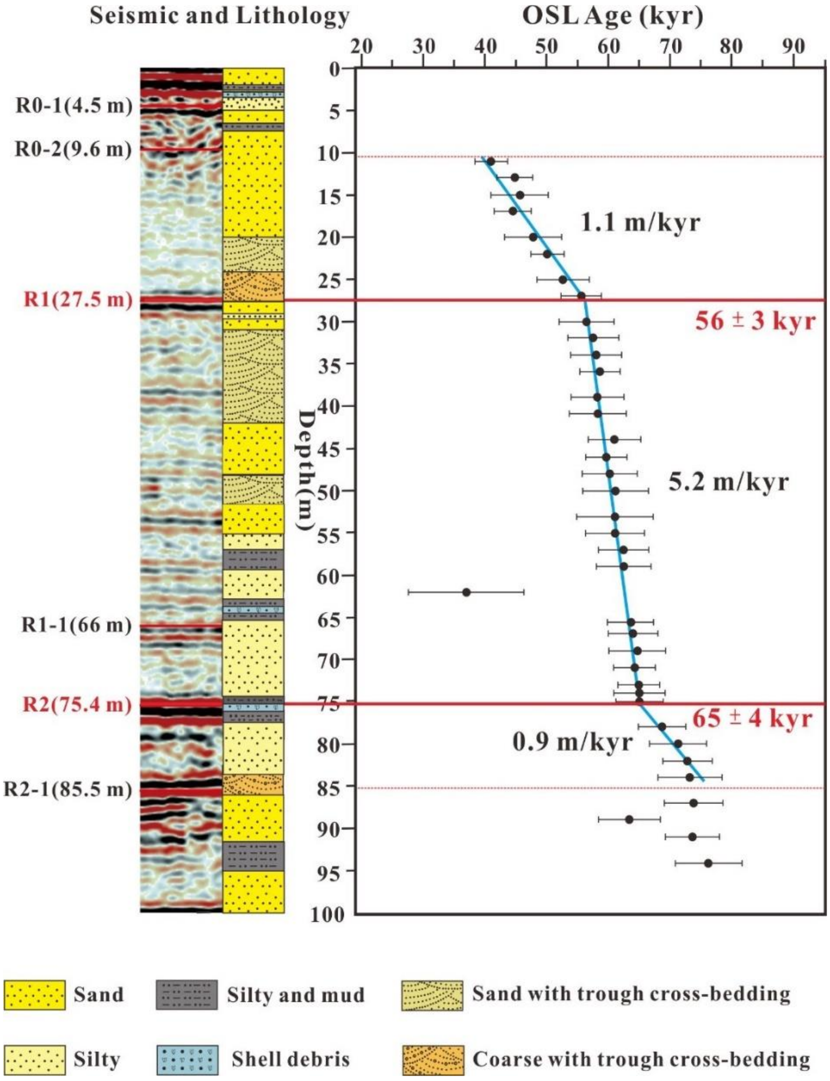

Figure 2. Coring profile at site ZBW, Beibu Gulf, showing the primary seismic reflectors, lithology, OSL sediment age data, and accumulation rates (modified from Feng et al. 2018b).

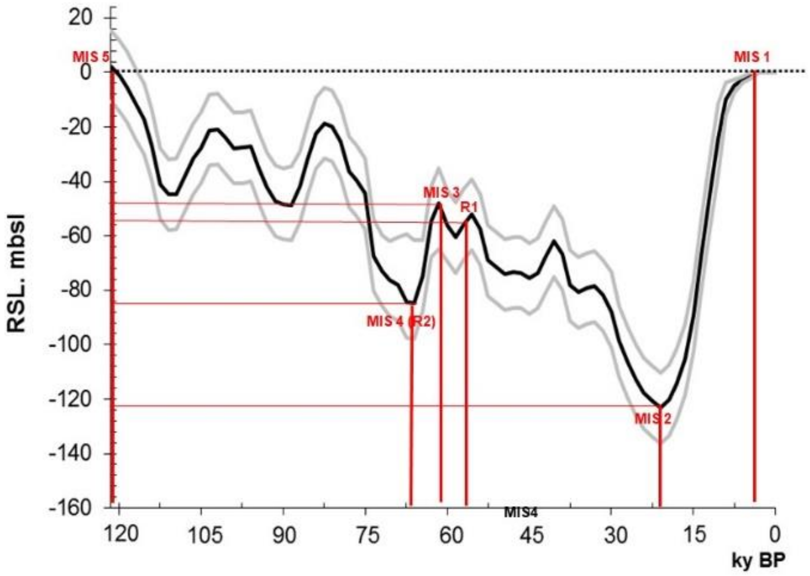

Figure 3. Global sea-level curve (modified after Waelbroeck et al., 2002). The mean is displayed by the bold black line and the grey curves show the corresponding confidence levels. Low-stand, respective high-stand of Marine Isotopic Stages 5 to 1 as well as the age of reflectors R1 and R2 (standing for MIS 4 sl low-stand) according to Table 1 are marked (x-axis) together with the related sea-level values (y-axis).

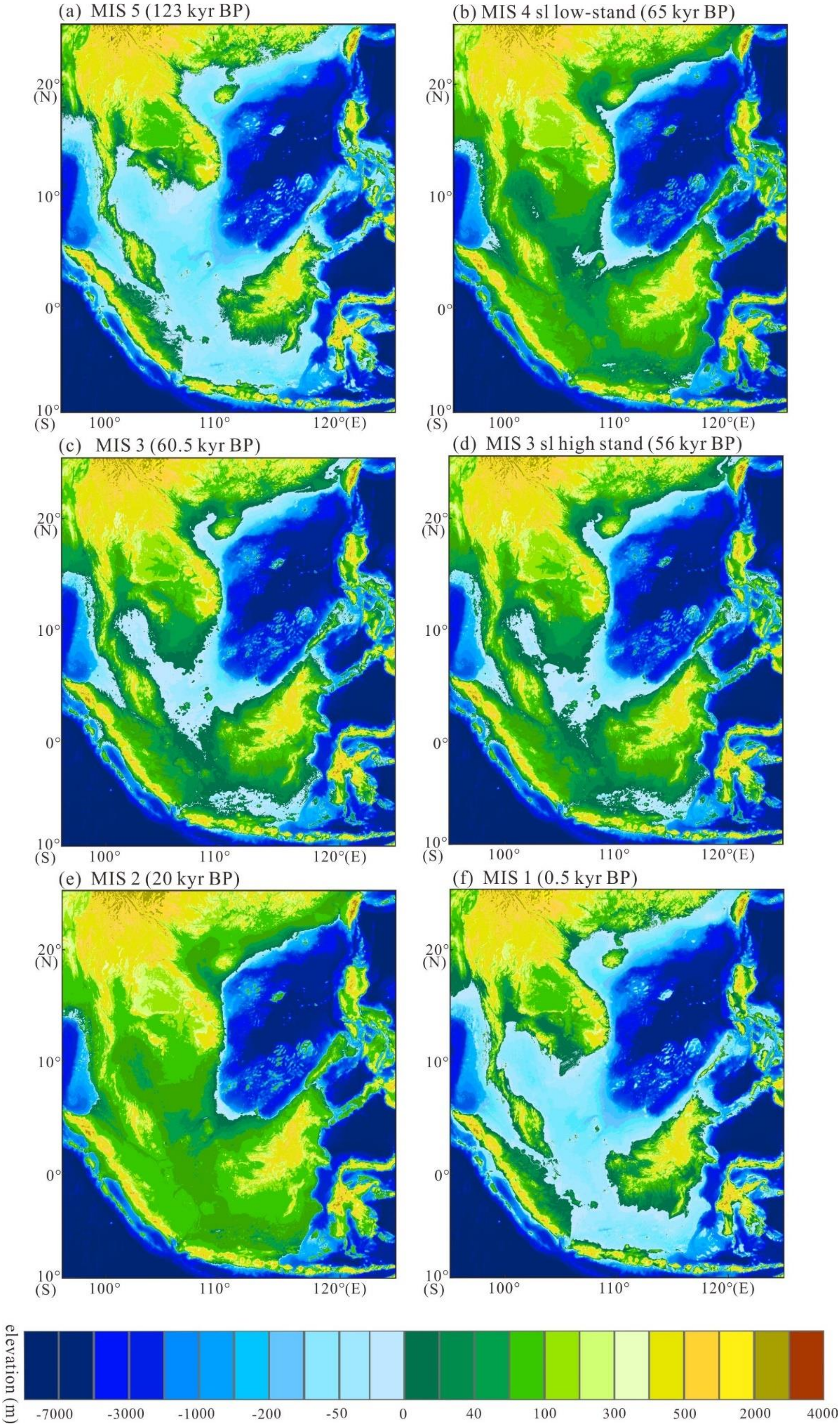

Figure 4. Paleogeographical map of the SCS and adjacent areas (regional scale) (a)

MIS 5, (b) MIS 4 sl low-stand (R2: 65 kyr BP), (c) MIS 3, (d) MIS 3 sl high-stand (R1: 56 kyr BP), (e) MIS 2, (f) MIS 1.

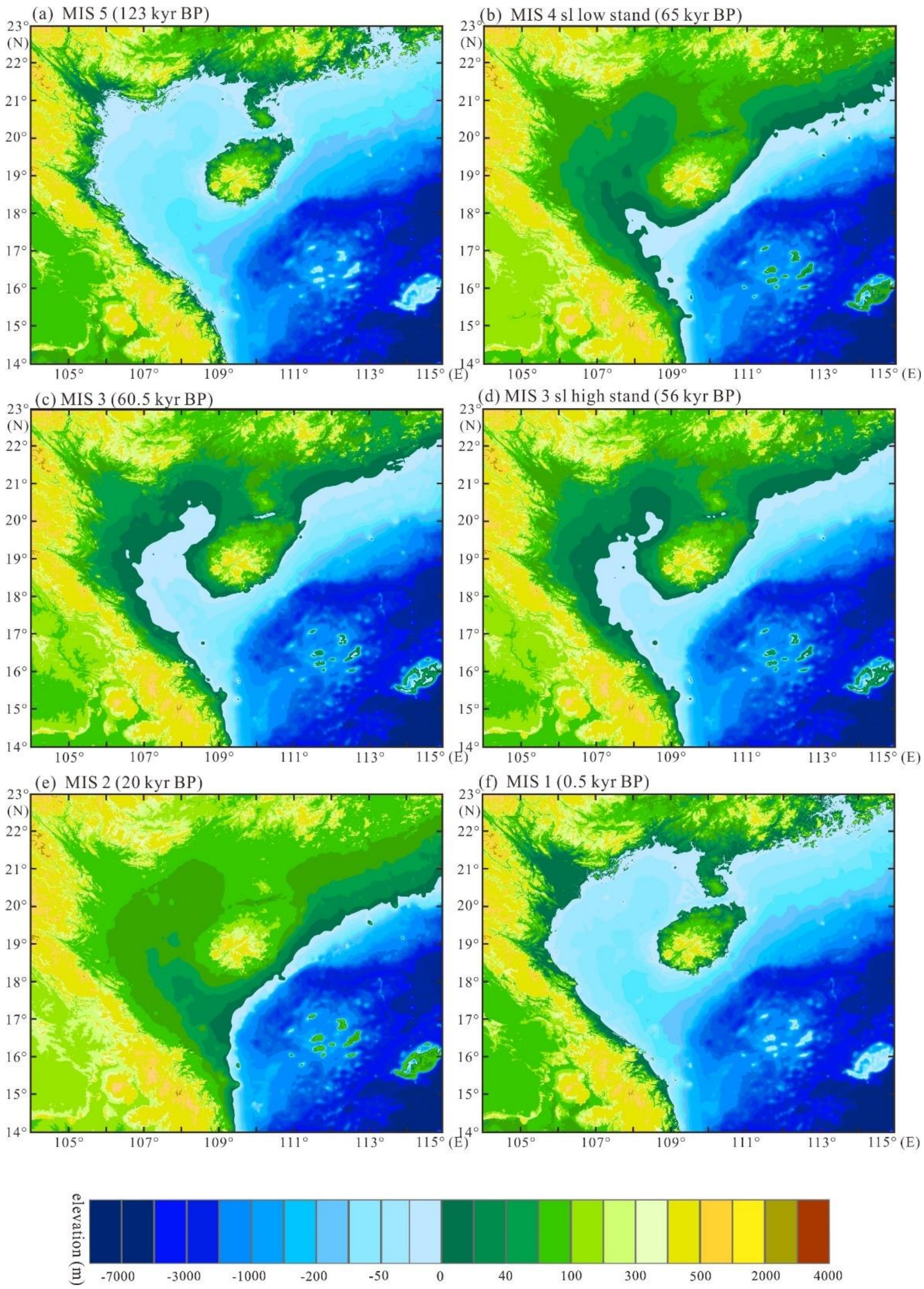

Figure 5. Paleo-geographical maps of the northwestern SCS and adjacent areas (local scale) (a) MIS 5, (b) MIS 4 sl low-stand (R2: 65 kyr BP), (c) MIS 3, (d) MIS 3 sl high-stand (R1: 56 kyr BP), (e) MIS 2, (f) MIS 1.

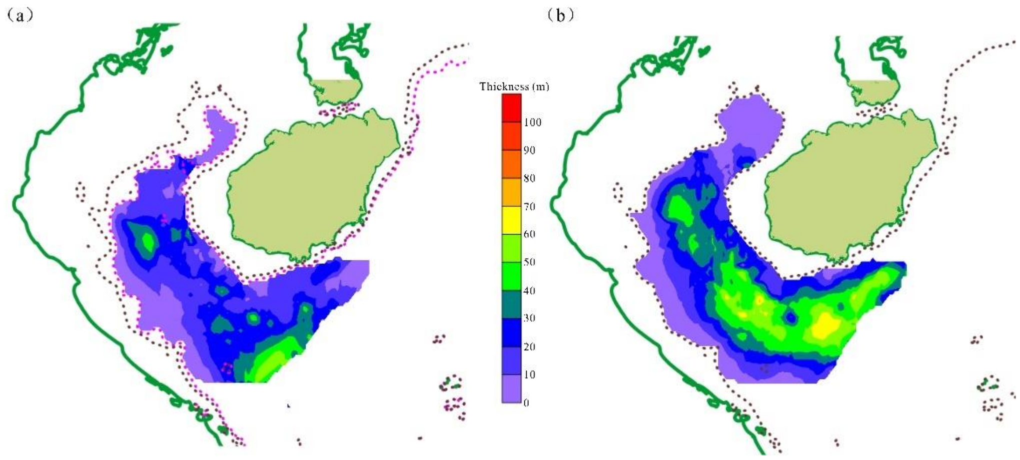

Figure 6. (a) *(ΔSED$_{R0-R1}$)* thickness of sediment unit (R0-R1) (scale in m),

(b) *(ΔSED$_{R1-R2}$)* thickness of sediment unit (R1-R2) (scale in m)

dark green solid line: recent coastline

dotted black line: paleo-coastline MIS3 sl high-stand, 60.5 ky BP

dotted purple line: paleo-coastline R1 (falling sl), 56 ky BP

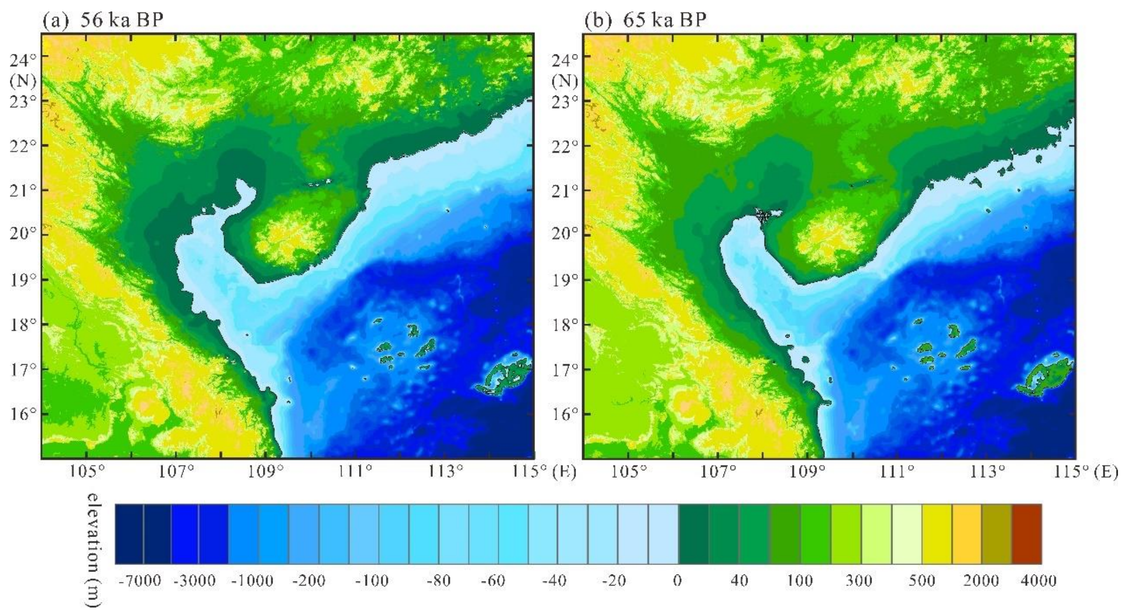

Figure 7. (a) Paleo-DEM$_{56kyBP}$ map, (b) Paleo-DEM$_{65kyBP}$ map

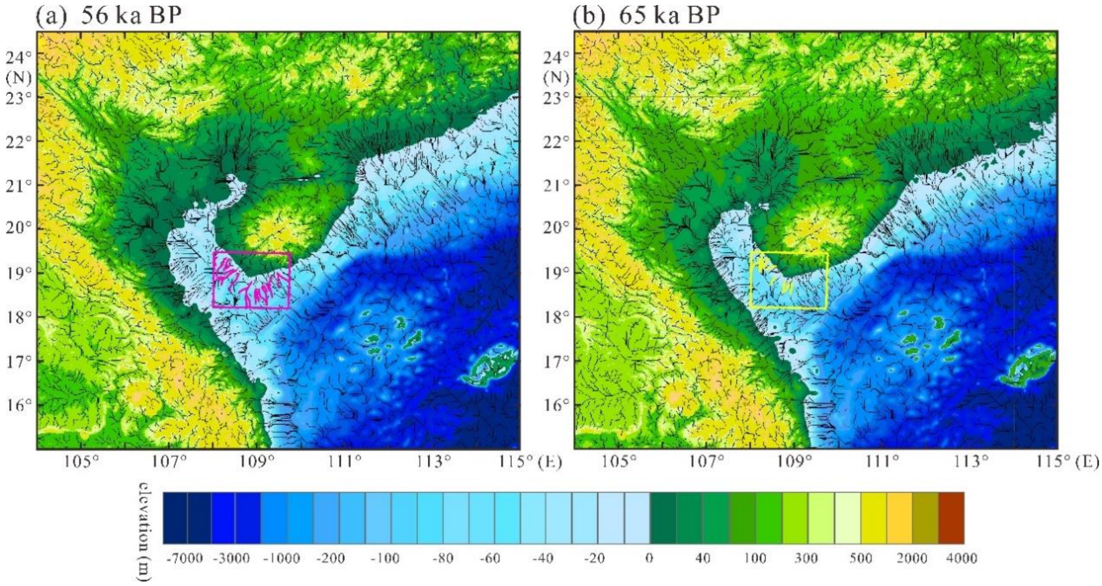

Figure 8. (a) Paleo-DEM$_{56kyBP}$ map superposed with paleo-valley axes and paleo-distributary channels generated by Miluch et al. (2020, this Special Issue) (b) Paleo-DEM$_{65kyrBP}$ superposed with paleo-valley axes and paleo-distributary channels generated by Miluch et al. (2020, this Special Issue)

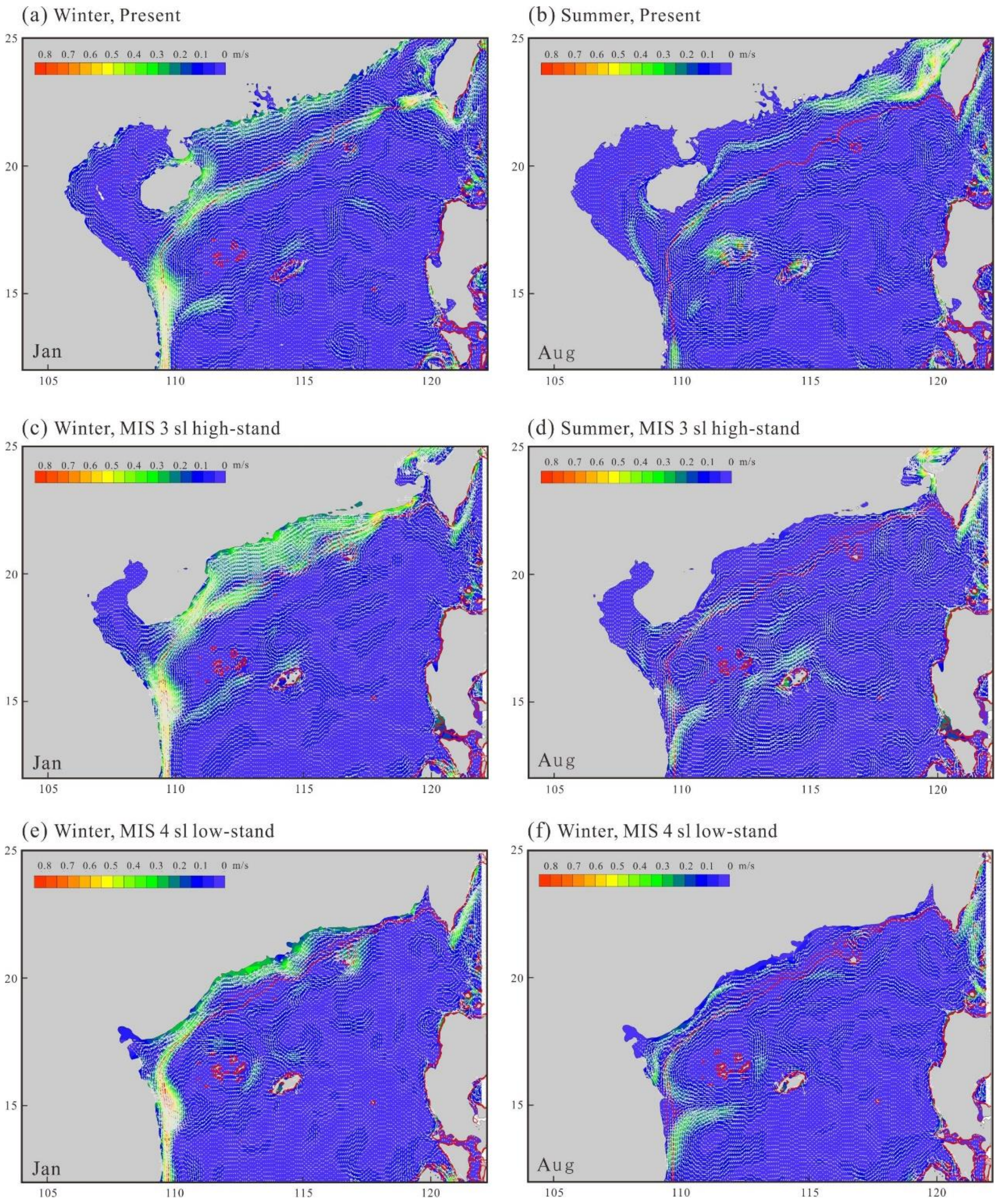

Figure 9. Simulated current (vertically-averaged and seasonally mean) of the northwestern SCS in (a) winter of the modern period, (b) summer of the modern period, (c) winter during MIS 3 sl high-stand, (d) summer during MIS 3 sl high-stand, (e) winter during MIS 4 sl low-stand. (f) summer during MIS 4 sl low-stand

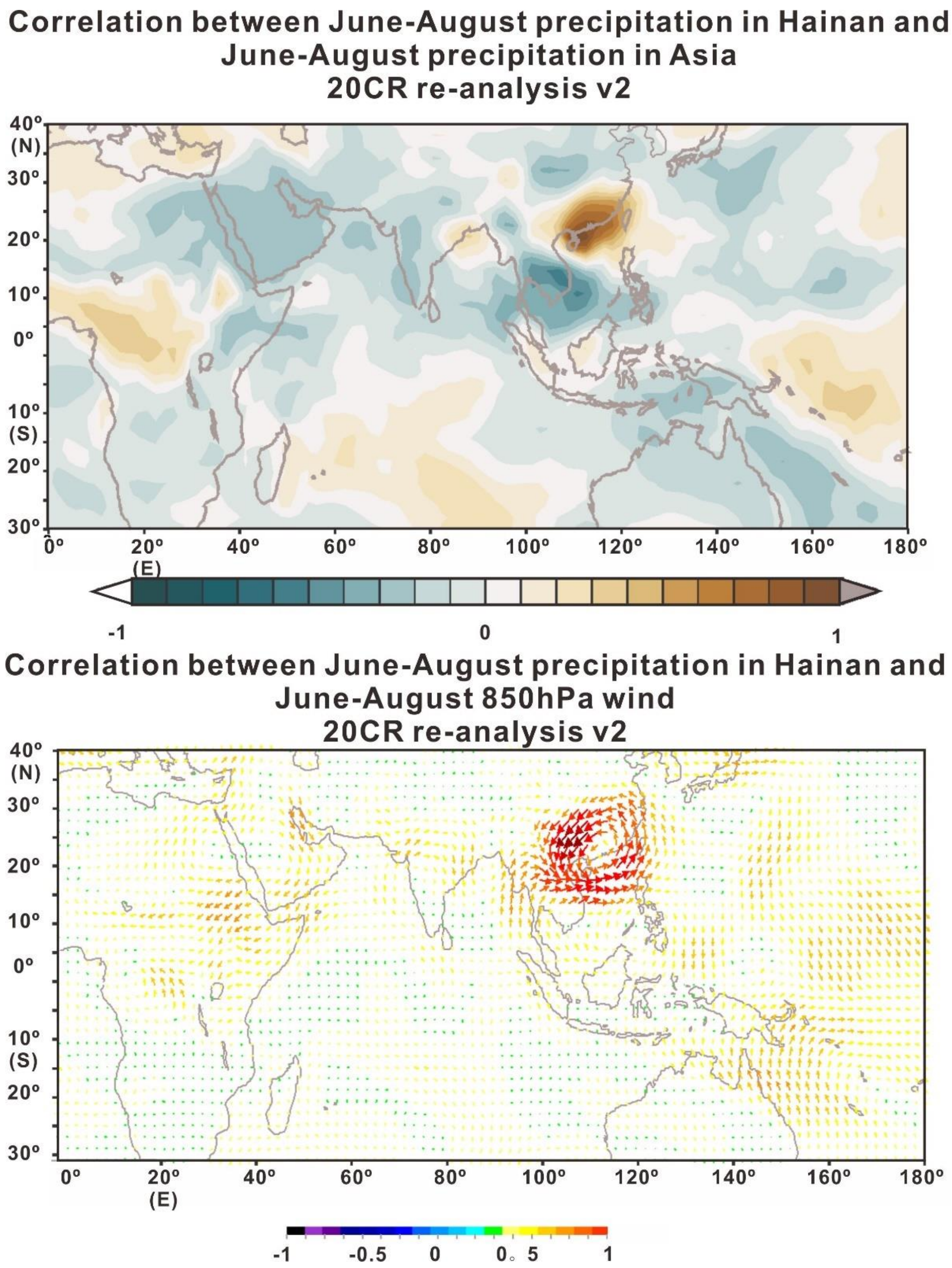

Figure 10. Results of re-analysis of meteorological data from 1871 to present.

(a) Correlation between June-August precipitation on Hainan island and June-August precipitation in Asia.

(b) Correlation between June-August precipitation on Hainan island and June-August precipitation in Asia and June-August 850h Pa wind.